AES/PE/10-30 *MODELING AND LABORATORY STUDY OF CARBONATED WATER FLOODING*

30-09-2010 *ARTHUR J.E. STEFFENS*

Department of Geotechnology

Delft University of Technology

Title	Modeling and Laboratory Study of Carbonated Water Flooding
Author	A.J.E. Steffens
Date	October 2010
Professor	Prof. Dr. P.L.J. Zitha
Supervisors	Prof. Dr. P.L.J. Zitha Dr. Ir. E.S.J. Rudolph
Graduation Committee	Prof. Dr. P.L.J. Zitha Dr. Ir. E.S.J. Rudolph Dr. Ir. C.W.J. Berentsen Prof. Ir. C.P. Van Kruijsdijk
TA Report Number	AES/PE/10-30
Postal Address	Section for Petroleum Engineering Department of Applied Earth Sciences Delft University of Technology P.O. Box 5028 The Netherlands
Telephone	(+31) 15 2781328 (Secretary)
Telefax	(+31) 15 2781189

ABSTRACT

Carbonated Water Flooding (CWF) is an enhanced oil recovery (EOR) method where an oil reservoir is flooded with water containing dissolved CO_2. It is being considered as a promising EOR (Enhanced Oil Recovery) method for maturing light and heavy oil fields. A numerical and experimental study of the CWF was conducted, focusing on the underlying physical phenomena.

In MATLAB, a numerical model describing a 1D CWF process was formulated assuming immiscible conditions. Modeling predictions have shown that in this simulator the oil swelling accounts for an increased oil production, together with a reduced residual oil saturation. This reduced residual oil saturation is the consequence of a reduced interfacial tension. However, the effect of this reduced residual oil saturation should be studied thoroughly.

In addition to the numerical model, core-flood experiments have been performed using Bentheimer sandstone and n-hexadecane to validate the model predictions. It was found that injecting water containing 3.7% CO_2 of the total mass of the aqueous phase reduces the residual oil saturation from pure water flooding to about 12.8. The experiment is performed with periods of injection and no injection, where an experiment with continuous injection would have provided more information about oil banking.

The results of the experiment have been used to validate the model. From this validation it is deducted that either the residual oil saturation is reduced if the CO_2 content in the oil phase is increased or there are errors in both the experiments and simulations. The mechanisms occurring during CWF are described (oil swelling, viscosity reduction, changing densities, solubility, changes in residual oil saturation).

PREFACE

This thesis was done as a part of the Master Petroleum Engineering of the Delft University of Technology.

Research has been performed in the past at the Delft University of Technology combining electromagnetic heating and CWF (Tran, et al., 2009). This study is a continuation with focus on CWF. The known literature has been studied and applied to perform thorough analysis of the subject, both experimental and numerical.

I would like to express my deepest gratitude towards everybody who helped me during my thesis work. Especially Pacelli Zitha and Susanne Rudolph, who supervised the complete project, provided input and guided me through the whole process. In addition to this I would like to thank Cas Berentsen and Cor van Kruijsdijk for showing interest in my research and willingness to be part of my thesis committee.

I would also like to thank all the technical laboratory staff who helped me in the laboratory, especially Henk and Henny who were always available for assistance and advice, but of course also Jolanda, Ellen, Karel and Jan.

A special thanks for Cas Berentsen, who took the time to help me unraveling the secrets of MATLAB.

A final thanks for my family and friends, who supported me during the whole period of graduation. Thank you for all the input, support, financial help, mental coaching, coffee/foosball breaks. You have been a great help whenever I needed it.

CONTENTS

LIST OF FIGURES

LIST OF TABLES

NOMENCLATURE

Symbol	Unit	Description
A	[m^2]	cross section area
a	[m^2]	internal radius of tip seal
C	[kg m^{-3}]	concentration
D	[kg m^{-1} s^{-}]	dispersion coefficient
D	[m^2 s^{-1}]	diffusion constant
F	[-]	fractional flow
G	[-]	geometric factor
g	[-]	Constant in the Hebach correlation
J	[kg m^{-2} s^{-1}]	diffusion flux
k	[m^2]	Permeability
L	[m]	length of the core
l	[m]	base of the triangular pore
MW	[gr mol^{-1}]	molecular weight
p	[bar]	Pressure
PV	[m^{-3}]	pore volume
q	[m s^{-1}]	flow rate
R	[kg m^{-3} s^{-1}]	reaction rate
r	[m]	Radius
S	[-]	Saturation
sf	[-]	sorting factor
sol	[mol mol^{-1}]	Solubility
t	[s]	Time
T	[K]	Temperature
u	[m s^{-1}]	darcy velocity
U	[kg m^{-3} s^{-1}]	mass transfer rate
V	[m^{-3}]	Volume
x	[m]	Distance
y	[-]	Emera and Sarma constant
A	[-]	Sensitivity analysis constant
γ	[-]	Specific gravity
Δ	[-]	delta (difference)
δ	[-]	Delta
λ	[m^2 Pa^{-1} s^{-1}]	phase mobility
μ	[pa s]	Viscosity
ρ	[kg m^{-3}]	Density
σ	[N m^{-1}]	interfacial tension
τ	[m]	mass transfer area per unit length of the core
φ	[-]	Porosity
χ	[-]	mole fraction

ω	[-]	mass fraction

Table 0-1: Nomenclature of symbols

Subscript	Description
1	1
2	2
b	bulk
b	bubble point
c	capillary
core	core
dead	dead volume
end	endpoint
g	gas
i	initial
inj	Injection/injected
ma	Matrix
max	maximum
o	oil
or	residual oil
prod	production/produced
r	relative
w	water
wc	connate water
we	efficient water
α	phase α

Table 0-2: Nomenclature of subscripts

Superscript	Description
CO_2	pure CO_2
o	pure oil
w	pure water
X	species

Table 0-3: Nomenclature of superscripts

1. INTRODUCTION

Over the lifetime of an oil reservoir, oil is usually recovered in three phases, namely primary, secondary and tertiary recovery. Primary recovery is characterized by natural flow of crude oil to the producer wells driven by the pressure drawdown across the reservoir. The recovery of oil in this stage is in the range of 5 – 20% of the Oil Initially In Place (OIIP). Secondary or Improved Oil Recovery (IOR) involves the injection of gas or liquids with the goal of pressure maintenance. The incremental oil recovery is 20 – 30%. The tertiary phase is also called Enhanced Oil Recovery (EOR). EOR methods can be divided into thermal methods (e.g. steam injection) and non-thermal methods. Non-thermal methods can be split up into chemical methods (e.g. polymer flooding, surfactant flooding) and non-chemical methods (miscible gas flooding). In many reservoirs, a large volume of oil ranging from 25-50% of the OIIP is left behind, even after EOR. There is thus need for processes that can improve the oil recovery for this kind of reservoirs.

Examples of IOR are the injection of gases such as nitrogen or CO_2 or Water-Alternating-Gas (WAG)-injection. A problem with these methods is that the sweep efficiency is still poor, so that this method is often not economically feasible. Figure 1-1 illustrates a possible explanation for the low sweep efficiency. Due to large density differences between the gas and either the oil and the water phase, gas override is observed. The injected gas rises upwards and moves past the oil, so that only a small portion of the oil in place gets in contact with the injected gas. By alternating the gas injection with water injection, it is intended to minimize the gas override. However, the sweep efficiency is still low. To overcome these problems, water with dissolved CO_2 is injected into the reservoir. This method is called Carbonated Water Flooding (CWF).

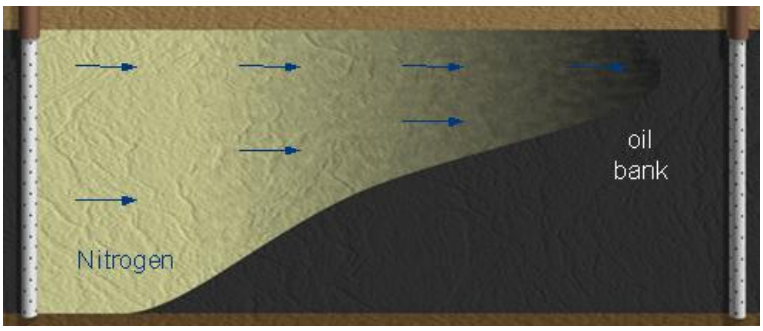

Figure 1-1: Illustration of the poor sweep efficiency of gas injection

This non-thermal tertiary recovery method is applied to enhance oil recovery from mature conventional oil or heavy oil reservoirs. A limited number of field trials and laboratory studies have proven that oil recovery is indeed improved by CWF (Nevers, 1964)(Tran, et al., 2009)(Riazi, et al., 2009). However, so far the method has not yet been applied routinely. CO_2 is used for this purpose because relatively large amounts of CO_2 can be dissolved in the water compared to other gases (Figure 1-2). CWF maximizes the contact area of CO_2 with the oil phase due to a better sweep efficiency.

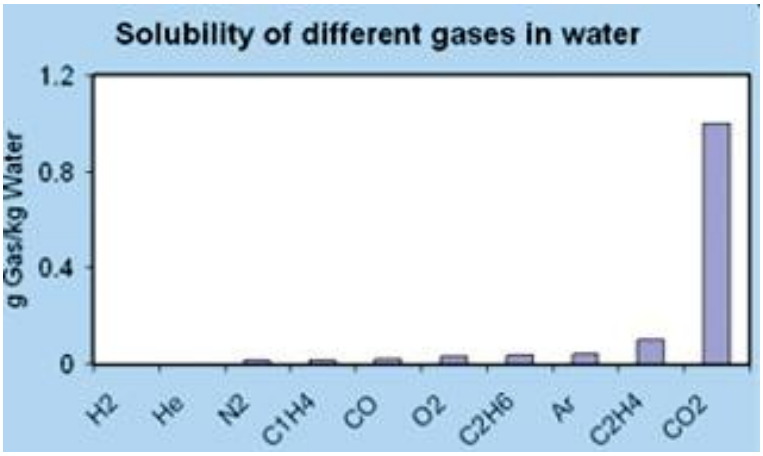

Figure 1-2: The storage potential for CO_2 in water compared to other gasses

When the aqueous phase contacts the oil phase, CO_2 is transferred from the water phase into the oil phase, initiating several mechanisms. De Nevers (1964) presented a Buckley-Leverett analysis of CWF as a secondary injection method, showing that oil swelling and viscosity reduction are responsible for the improved oil recovery. According to Riazi et al (2009) and Tran et al (2009) another effect of injecting CO_2 is that the interfacial tension (IFT) between the oil and the aqueous phase is reduced. With this information, the general principles of CWF are known but a detailed description of the mechanisms is still missing.

The hypothesis is that the incremental oil recovery is obtained due to the mass transfer of CO_2 from the water phase into the oil phase, causing oil mobilization because of oil swelling, viscosity reduction and a reduced IFT, which results in a decreased irreducible oil saturation.

The goal of this study was to investigate if the residual oil after application of water flooding can be recovered by applying CWF, thus lowering the irreducible oil saturation. Additionally, the underlying mechanisms responsible for the improved oil recovery are intended to be identified. The approach applied for this study, is first to set up a model which describes a CWF. Thereby, a number of assumptions are made. Then experiments are performed to verify the results of this model.

In the numerical model describing the process of CWF, it was accounted for the changes in the composition of the oil and the water phase due to mass transfer from the carbonated water into the oil phase and vice versa. A number of sensitivity analyses have been performed to identify the impact of the following parameters: Number of grid blocks, time step, injection rate, maximum solubility of CO_2 in oil, pressure, residual oil function, diffusion constant, viscosity and the density of the oil phase.

Preliminary experiments have been performed to show if oil recovery is really improved by injecting carbonated water after a water flooding. In a next step, the experimental data were used to validate the model. Based on the comparison of the experimental and modeling data it can be identified which of the made assumptions are realistic. This then allows to get a better understanding of the mechanisms occurring during CWF, to a certain degree.

As a last step, based on the results and experiences of the simulations and the experiments, a number of recommendations were formulated for further research in this field.

The set-up of the thesis is as follows. First a short introduction to the subject, the potential, the challenges and the goals of the research are presented. In the second chapter, the theory necessary to understand the numerical simulation, experiments, results and the discussions is given. Then the numerical model is presented. This chapter is followed by a description of the experimental work. In chapter 5 the results are presented and discussed. Finally, the last chapter describes the conclusions and recommendations.

2. BACKGROUND

In this chapter the background information for the reported research work is given. The following paragraphs describe phase behavior, IFT phenomena and mass transfer. In the last paragraph the attention is turned to the flow through porous media. Finally a short paragraph is devoted to an existing Buckley-Leverett theory for the description of CWF.

2.1 PHASE BEHAVIOR

In this study three components are present during the CWF, namely oil, water and CO_2. The phase behavior of the mixtures in the porous medium must be understood to allow analysis of the processes occurring during CWF. The phase behavior can be derived from pressure, composition-diagrams such as given in Figure 2-1. The left illustration shows the composition of the aqueous phase the water – CO_2 system at constant temperature. The right illustration (Kobayashi, et al., 1986) shows the phase behavior of the hexadecane – CO_2 system at constant temperature.

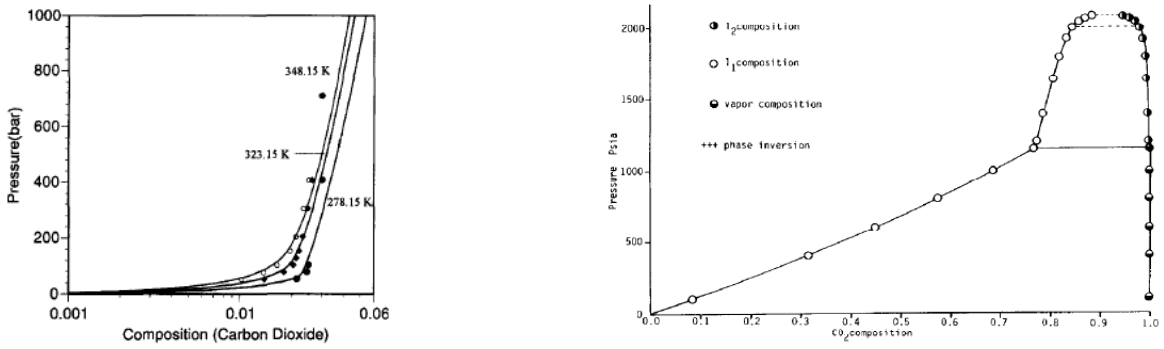

Figure 2-1: p,x-diagrams of the water - CO_2 mixture (left) and the n-hexadecane – CO_2 mixture (right)

For both systems, the solubility of CO_2 in the respective component, water or hexadecane, increases; with increasing with increasing pressure; while it decreases with increasing temperature. In general, CO_2 tends to be dissolved in the organic phase more easily than in the aqueous phase. Thus, it can be assumed that CO_2 is transferred from the carbonated water phase into the oil phase when injecting carbonated water into a reservoir.

The distribution of CO_2 over the water and the hexadecane phase can be described by the so-called k-value, or distribution coefficient. Values for the distribution coefficients can either be computed with an appropriate equation of state, or taken from experimental or literature data or computer by correlations. This distribution coefficient describes how much CO_2 can be dissolved in the oil compared to the CO_2 which is dissolved in the water. If it is assumed that hexadecane and water do not mix, the k-values can be deducted from the phase behavior of the binary system water + CO_2 and hexadecane + CO_2.

$$k = \left[\frac{\omega_{CO_2}^{w}}{\omega_{CO_2}^{o}} \right]_{p,T} \quad (2\text{-}1)$$

In general, the solubility of CO_2 is a function of pressure, temperature and API gravity (Emera, et al., 2006). Emera and Sarma (2006) have defined correlations, (2-2) and (2-3), to describe the solubility of CO_2 in the oil phase as function of temperature, pressure, the oil gravity and the molecular weight of the oil. These correlations are valid for subcritical conditions (Emera, et al., 2006).

$$x_o^{CO_2} = 2.238 - 0.33y + 3.235y^{0.6474} - 4.8y^{0.25656} \quad (2\text{-}2)$$

$$y = \gamma \left(0.006897 \frac{\left(1.8T + 32^{0.8}\right)}{p} \right)^{\exp\left(\frac{1}{MW}\right)} \quad (2\text{-}3)$$

Herein χ is the mole fraction of CO_2 in the oil phase, γ the specific gravity of the oil, T the temperature, p the pressure and MW the molar weight of the oil.

The amount of CO_2 that can be dissolved in water at a given temperature and pressure (appendix A) is calculated with the model of Diamond (Diamond, et al., 2002), which is valid up to 373 K and 100 MPa.

2.1.1 FLUID DENSITIES

For the description of the density of the aqueous phase fully saturated with CO_2, the correlation of Hebach et al (2004) was used (2-4). The correlation has a validity regime between 1 and 30 MPa and between 284 and 332 Kelvin (see also Figure 2-2).

The solubility of CO_2 in water is reduced by 30% for every 100.000 ppm of total dissolved solids (Whitson, et al., 2000). In this work, the salinity of the aqueous solution is 20.000 ppm. Because of the relatively low salinity it can be assumed that the solubility of CO_2 in the aqueous phase is not affected due to dissolved salt. In Figure 2-2 the change in density of brine saturated with CO_2 as function of pressure at one arbitrarily chosen temperature of 293 K is given computed using equation (2-4):

$$\rho_w = g_0 + g_1 p + g_2 T + g_3 p^2 + g_4 T^2 + g_5 pT + g_6 p^3 + g_7 T^2 p + g_8 T p^2 \quad (2\text{-}4)$$

Here ρ_w is the density of the aqueous phase, g_0 to g_8 are constants, T the temperature and p the pressure.

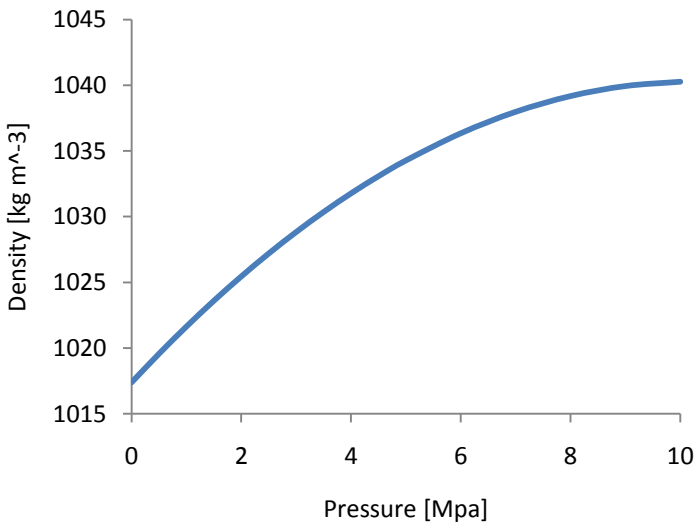

Figure 2-2: The density of brine saturated with CO_2 as function of pressure at a temperature of 293 K. This correlation is computed with equation (2-4)

According to DeRuiter (1994) the density of oil increases with increasing CO_2-content. Emera and Sarma (2006) suggested a correlation, (2-5) and (2-6), for the description of the oil density based on the amount of dissolved CO_2. For the simplicity of the model a simplified linear correlation has been created (2-7) based on the Emera and Sarma correlation. This equation is purely a function of the oil phase composition and not of pressure as the original equation by Emera and Sarma. In this equation the constants represent the densities of hexadecane and CO_2 at the given pressure and temperature. Both functions are displayed in Figure 2-3. For the simulations equation (2-7) was used.

$$\rho_o = \rho_i - 0.10276y^{0.608} + 0.1407y^{0.6133} \quad (2\text{-}5)$$

$$y = \frac{\gamma\rho_i(p - p_b)^{1.25}}{1.8T + 32} \quad (2\text{-}6)$$

$$\rho_o = 773.19 + 21.826\omega_o^{CO_2} \quad (2\text{-}7)$$

In these correlations, ρ_o is the density of the oil phase, ρ_i is the density of the pure (or initial) oil, ω the mass fraction CO_2 dissolved in the oil, p and p_b are respectively the pressure and bubble point pressure of the oil and γ the specific gravity of the oil.

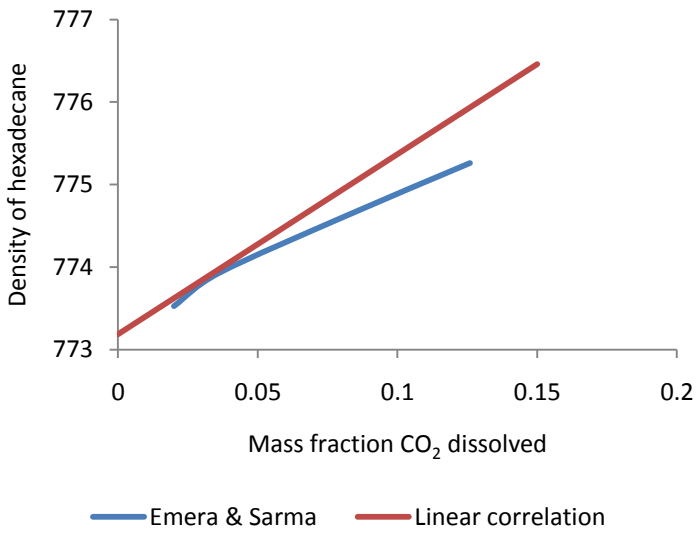

Figure 2-3: Density of hexadecane as a function of dissolved CO_2 at a temperature of 293 K and a pressure of 25 bar. The curves are calculated by the correlation of Emera and Sarma, (2-5) and (2-6) and a linear correlation (2-7)

2.1.2 Oil Swelling

The oil swelling factor is defined as the ratio of CO_2 saturated oil to oil volume at a given temperature and pressure. When CO_2 dissolved in oil, an increase in liquid volume occurs (Simon, et al., 1965). Thereby, the oil swelling is influenced by the interactions between the dissolved CO_2 and the oil.

Assume that the residual oil saturation is the same whether the oil is carbonated or not. Then the same oil volume will contain less pure oil if it is carbonated, due to oil swelling (Nevers, 1964).

2.2 Interfacial Tension

The interfacial tension between two phases is a crucial parameter for flow through porous medium. Thereby, the interfacial tension is a measure for the strength of interfacial forces. The interfacial tension between two phases in porous medium determines, among others, how much oil can be produced from a water-wet porous medium. In this work, the influence of IFT is not incorporated directly into the model but by assuming that with an decreasing IFT the residual oil saturation decreases. Thereby, it is assumed that the CO_2 content in the oil and aqueous phase affects the IFT between these two phases (Riazi, et al., 2009), and that therefore the residual oil saturation is reduced.

2.3 Mass Transfer

When applying CWF, CO_2 will be transferred from the aqueous phase into the oil phase and vice versa. As long as a driving force, e.g. the difference in chemical potential, is present, mass will be transferred from one phase into another (Wesselingh, et al., 1990). If the contact area (IFT area)

of the two phases is large, more mass can be transferred across the interface (Helland, et al., 2006).

In this work, the mass transfer is described by the two liquid film theory (Figure 2-4). At the left hand side of the interface the aqueous phase is situated, at the right hand side the oil phase. Here the situation is displayed at the initial time and on the long term. In the beginning the concentration in the water is higher than in the oil so that mass transfer from the aqueous phase to the oil phase occurs. The maximum possible mass transfer is determined by the phase equilibrium, the distribution coefficient k. Thus, when equilibrium is reached, the concentration difference of CO2 in the aqueous and organic phase does not become zero.

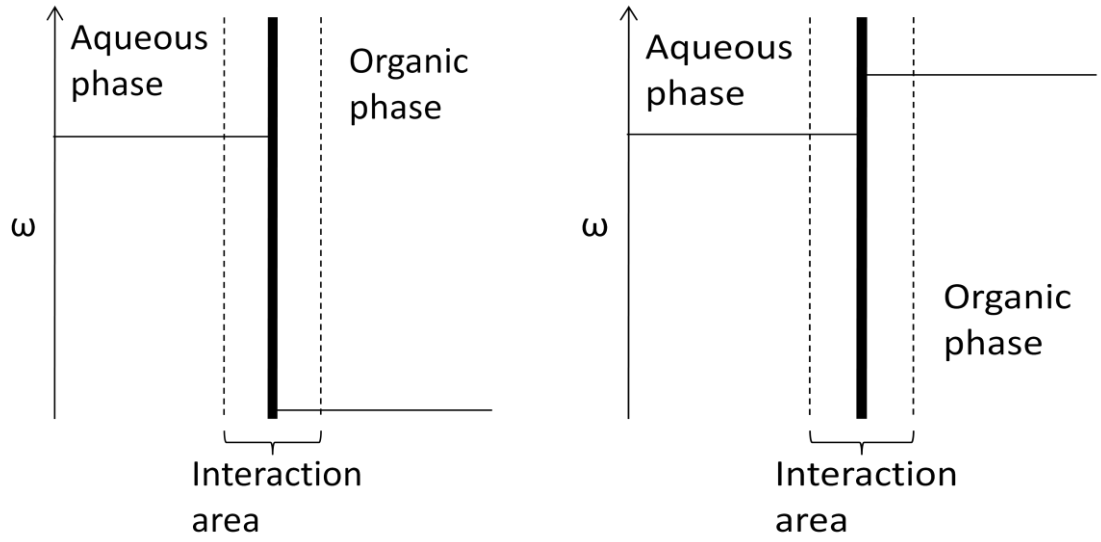

Figure 2-4: CO_2 concentration as a function of distance. The thick slap displays the interface. At the left hand side of the interface is the aqueous phase, at the right hand side the oil phase.

From above arguments a simple formula for the mass transfer rate can be written per phase:

$$U = J\frac{\tau}{A} \qquad (2\text{-}8)$$

Where U is the mass transfer rate, τ is the mass transfer active area per unit length of the medium and A the area of the cross-section of the core. J is a diffusion flux and can be formulated as (Treybal, 1980):

$$J = D\frac{\Delta C^{co_2}}{\Delta r} \qquad (2\text{-}9)$$

In this equation, D is the diffusion coefficient of CO_2 in the respective phase, Δr the distance between the bulk, either water phase or oil phase and the interface.

In the proposed model, the mass transfer between the oil and the aqueous phase is described by a simplified model in which a correction factor k is incorporated. The correction factor k accounts for the fact that mass transfer does not continue until the concentration difference in the two phases is equal to zero. Thus, the correction factor k is actually the distribution factor K.

$$\Delta C^{co_2} = k \cdot C_o^{co_2} - C_w^{co_2} = k \cdot \rho_o \omega_o^{co_2} - \rho_w \omega_w^{co_2} \quad (2\text{-}10)$$

In this investigation, the k-value has been derived from the (maximum) solubility of CO_2 in either the oil (2-2) and the water phase, resulting in a k-value of approximately0.35.

2.4 Flow in Porous Media

2.4.1 Modeling of the Residual Oil Saturation

The residual oil saturation defines the volume of oil that cannot be produced from a reservoir. It is assumed that the IFT affects the residual oil saturation. According to Stegenmeier (1977) the residual oil saturation decreases with increasing capillary number (see Figure 2-5).

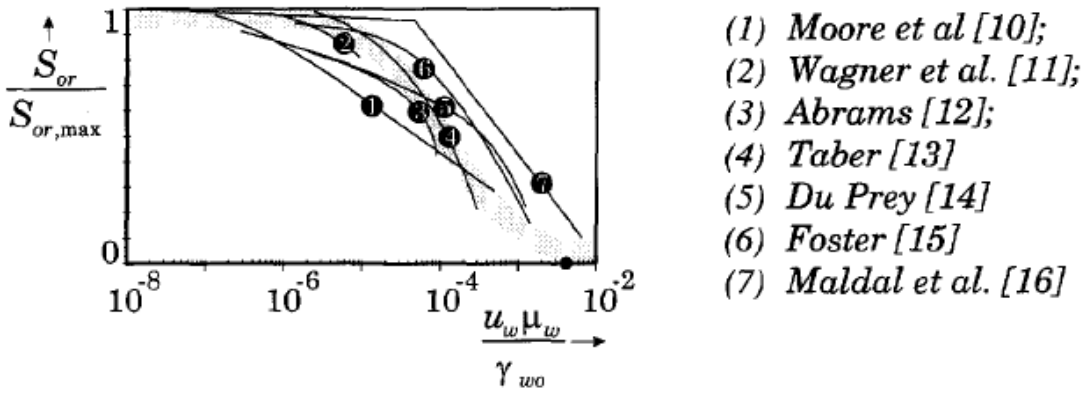

Figure 2-5: Normalized residual oil saturation as function of capillary number in 'homogeneous' rock (Stegenmeier, 1977).

The capillary number is a function of the water velocity, water viscosity and the IFT between the water and oil phase. If it can be assumed that the water velocity and viscosity are constant, the capillary number is only a function of the IFT.

$$N_{c,pore} = \frac{u_w \mu_w}{\gamma_{ow}} \quad (2\text{-}11)$$

The capillary number is small for high values for IFT, and the residual oil saturation is equal to the maximum oil residual saturation. The interfacial tension between the aqueous and the oil phase decreases when CO2 is dissolved in these phases. However, no experimental data exist to support this hypothesis.

To investigate the influence of changing IFT on the oil production when applying carbonated water flood, it is assumed that the residual oil saturation decreases and eventually approaches zero as the interfacial tension approaches zero.

An empirical equation is used to describe the residual oil saturation as function of dissolved CO_2 (see figure 2-6). The curves are displayed up to the maximum solubility of CO_2 in oil.

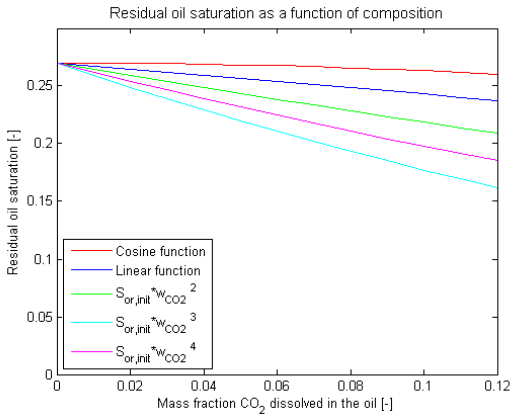

Figure 2-6: Residual oil saturation functions as a function of CO_2 mass fraction in the oil phase. Functions are empirically.

2.4.2 MOBILITY AND VISCOSITY

The mobility of a phase equation is a function of absolute permeability k, relative permeability k_r to this specific phase and its viscosity μ. With the mobility λ of oil and water the fractional flow f of oil and water can be calculated. The mobility of the oil and aqueous phase is described by:

$$\lambda_o = \frac{kk_{ro}}{\mu_o};\ f_o = \frac{\lambda_o}{\lambda_o + \lambda_w} \qquad (2\text{-}12)$$

$$\lambda_w = \frac{kk_{rw}}{\mu_w};\ f_w = \frac{\lambda_w}{\lambda_o + \lambda_w} \qquad (2\text{-}13)$$

According to Nissan and Grunberg (1949), the viscosity of an oil decreases with increasing amount of dissolved CO_2. In this work, the correlation as suggested by Nissan and Grunberg is used to describe the viscosity of the oil phase.

$$\log \mu = \omega_o^{'co_2} \log \mu_o^{co_2} + \omega_o^{'o} \log \mu_o^{o} + G\omega_o^{'co_2}\omega_o^{'o} \qquad (2\text{-}14)$$

G is the interaction parameter. The correlation is illustrated in Figure 2-7. Three viscosity functions are plotted to illustrate the effect of dissolved CO_2 on oil for different values of G. The curve for $G=0$ describes the ideal case, meaning the interactions between the CO_2 and the oil are uniform. An increasing value of G means that the interactions increase and are attractive.

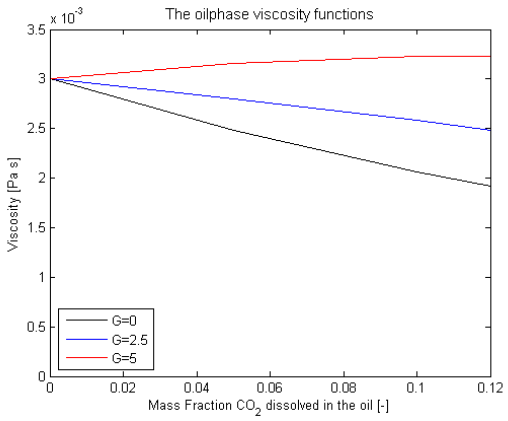

Figure 2-7: The viscosity of the oil phase as a function of composition. The curves are computed using the correlation of Nissan and Grunberg (2-14)

2.5 BUCKLEY LEVERETT ANALYSIS OF CWF

Nevers (1964) presented a Buckley-Leverett analysis of CWF in a porous medium containing oil and water at irreducible water saturation. In this analysis it was accounted for oil swelling and oil viscosity reduction. The effect of CO_2 on neither the IFT between oil and water, nor the influence of CO_2 on the density of these phases, was incorporated.

The changes in the oil recovery and water saturation compared to a water flood is due to the mass transfer of CO_2 from the water into the oil phase. When injected carbonated water gets in contact with the oil in a porous medium, CO_2 is transferred to the oil, because the solubility of CO_2 in oil is much higher than the solubility of CO_2 in water. The distribution of CO2 over the water and the oil phase at a given temperature and pressure is determined by the so-called distribution coefficient K describing the phase equilibrium.

In Figure 2-8 the cumulative oil and Co2 production and the water saturation and the CO2 concentrations in the reservoir for a plain water flooding and a CWF are given. From this graph it is clear that the cumulative oil production is higher when injecting carbonated water instead of pure water (Figure 2-8-d). In Figure 2-8-a it is illustrated how the water first propagates with a constant CO_2 concentration (G – E). The water saturation here is higher than the water saturation of the plain water flood. The additional oil produced from this area flows forward and forms an oil bank (C – B). This oil contains no CO_2. The section (E – C) is the carbonated zone. The difference between a plain water flood and a CWF is also illustrated in Figure 2-8-D, where the oil production is similar up to point B. Between points (B – E) the additional oil is recovered . Figure 2-8-c illustrates the cumulative production of CO_2.

Assume that the total amount of CO_2 injected is the projection on the y-axis of point D (see figure 2-9-c) . Then this will also be the point that the CWF process will stop and no more CO_2 will be produced.

As a reason for the decreased residual oil saturation (difference between F and G), De Nevers gives the swelling-followed-by-shrinking-method. This method implies two processes. The first process is oil swelling due to dissolution of CO2 in the oil. The oil becomes more mobile and producible so that the oil saturation increases when applying CWF. The second process is oil shrinking. This is due to the plain water flood which follows the carbonated water flood. The injected pure water extracts the CO_2 from the oil phase so that the oil shrinks. The oil shrinking results even in an oil saturation lower than the initial residual oil saturation.

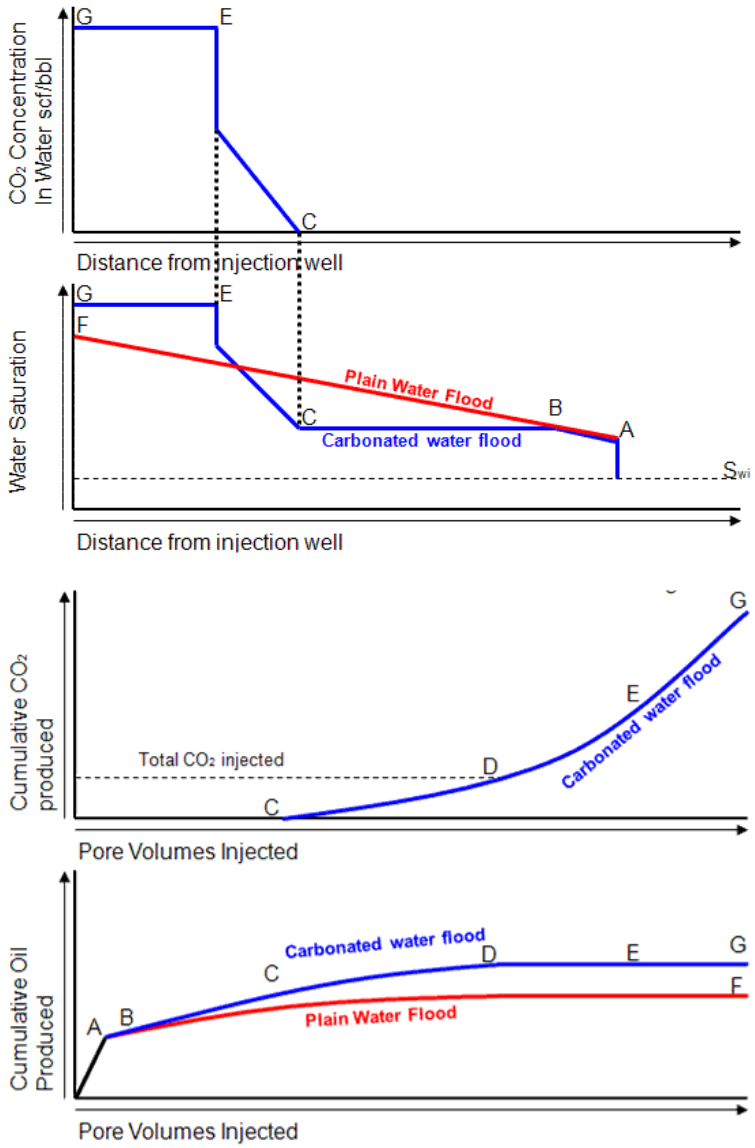

Figure 2-8: Comparison of plain water flood and CWF according to Buckley-Leverett theory by De Nevers (1964). From top to bottom: a) CO_2 concentration as a function of distance from injector; b) Water saturation as a function of distance; c) Cumulative CO_2 production as function of injected pore volume; d) Cumulative oil production as function of injected pore volume

3. MODEL FORMULATION

This chapter provides the formulation of the model. The first part of this chapter will cover the framework of the simulator. The second subchapter will discuss the formulation of the model. Finally, the modeling of the mass transfer is described.

3.1 FRAMEWORK

3.1.1 PHYSICAL MODEL

To model the CWF process we consider a homogeneous and isotropic porous medium with length L, cross-sectional area A, constant porosity φ and constant permeability k. The core is initially saturated with both water and oil, oil being at the residual oil saturation. Water with a mass fraction χ of 3.7% CO_2 is injected in the core at a flow rate q. In the core mass transfer will take place. We are concerned with the evolution of the distribution of saturations in the core and of the composition of the effluents in the core. From the core a water phase and an oil phase are produced.

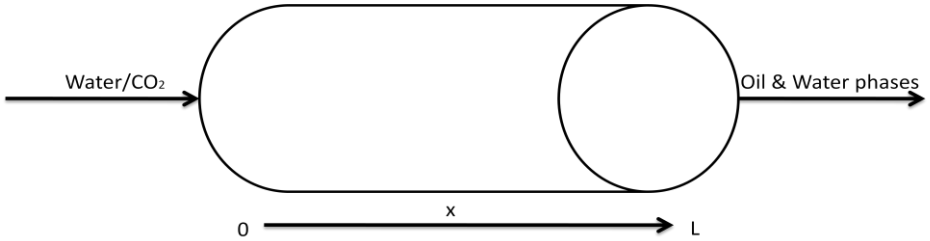

Figure 3-1: Injection of carbonated water in a horizontal cylindrical core

3.1.2 ASSUMPTIONS

- The model is 1-dimensional and gravity is neglected;
- No chemical reactions resulting from the formation of carbonic acid and its subsequent dissociation (3-1) are considered:

$$2H_2O + CO_2 \longleftrightarrow HCO_3^- + H_3O^+ \qquad (3\text{-}1)$$

- The dispersion in this process is negligible compared to the flow term because the medium is assumed to be well-homogeneous in terms of porosity and permeability;
- The porous medium is water wet;
- Two phases, water and oil, are present (no free gas); these are not soluble in each other;
- The IFT is incorporated into the model by describing the residual oil saturation as function of composition; with increasing CO_2 concentration in the oil the residual oil saturation decreases;
- The viscosity of the water phase is assumed constant.

3.2 FORMULATION

3.2.1 MASS BALANCE EQUATION

The main equation to derive the equations to describe the carbonated water flood as a 1D problem is the mass balance equation for all components in all phases. In general, for species *X* in phase *α* the mass balance can be written as:

$$\phi \frac{\partial(\rho_\alpha S_\alpha \omega_\alpha^X)}{\partial t} + \nabla\left(u_\alpha \rho_\alpha \omega_\alpha^X - S_\alpha D_\alpha^X \nabla \omega_\alpha^X\right) = U + \phi S_\alpha R_\alpha^X \quad (3\text{-}2)$$

The terms on the left hand side are respectively the accumulation term, the convective flow and the dispersion. The terms on the right hand side represent the mass transfer and reaction terms. *'U'* is the absolute value of mass CO_2 transferred from the water phase into the oil phase and has a positive value as long as the mass is transferred in this direction.

The set of equations can be rewritten for the mass balance equation (3-2) for every component in the system. As mentioned in the assumptions, the reaction and diffusion terms can be neglected. The relations for the oil phase are (3-3) and (3-4) and for the water phase (3-5) and (3-6). The system is solved for the pressure, saturation and composition in appendix C.

$$\phi \frac{\partial(\rho_o S_o \omega_o^o)}{\partial t} = -\nabla \cdot (u_o \rho_o \omega_o^o) \quad (3\text{-}3)$$

$$\phi \frac{\partial(\rho_o S_o \omega_o^{co_2})}{\partial t} = -\nabla \cdot (u_o \rho_o \omega_o^{co_2}) + U \quad (3\text{-}4)$$

$$\phi \frac{\partial(\rho_w S_w \omega_w^w)}{\partial t} = -\nabla \cdot (u_w \rho_w \omega_w^w) \quad (3\text{-}5)$$

$$\phi \frac{\partial(\rho_w S_w \omega_w^{co_2})}{\partial t} = -\nabla \cdot (u_w \rho_w \omega_w^{co_2}) - U \quad (3\text{-}6)$$

3.2.2 DARCY VELOCITY

The flow through porous media can be described by Darcy's law. The Darcy velocity *u* of the oil and water phase is a function of the oil and water phase mobility, λ_o and λ_w, and pressure drop *Δp over distance Δx*.

$$u_o = -\lambda_o \frac{\partial P_o}{\partial x} \quad (3\text{-}7)$$

$$u_w = -\lambda_w \frac{\partial P_w}{\partial x} \quad (3\text{-}8)$$

3.2.3 BOUNDARY AND INITIAL CONDITIONS

The porous medium is assumed to be a cylindrical core where only the inlet and outlet are open to flow i.e. no flow occurs across the cylindrical wall. The length equals 17 cm and the radius is 0.019 cm.

The amount of water present initially in the core is S_{wi}. The pore space is assumed to contain fluids at a fixed uniform pressure p_i. The amount of CO_2 dissolved in the fluids is defined by ω and is constant over the length of the core.

The constraint at the inlet surface is a fixed flow rate and for the outlet an extrapolated saturation. The boundary and initial conditions are summarized in Table 3-1 below.

Initial conditions	**Boundary conditions**
$p(x,0) = p_i$	$q_\alpha(0,t) = q_{\alpha,inj}$
$S_w(x,0) = S_{w,i}$	$S_w(L,t) = S_w(L,t-1) + ½ [S_w(L-1,t-1)-S_w(l,t-1)]$
$\omega_\alpha^{CO_2}(x,0) = \omega_{\alpha,i}^{CO_2}$	$\omega_\alpha^{CO_2}(0,t) = \omega_{\alpha,inj}^{CO_2}$

Table 3-1: Table with boundary and initial conditions

Numerical control in the model is necessary to prevent any unrealistic solutions. These consist of the sum of the saturation, sum of the relative permeabilities and sum of the mass fractions in the different phases:

$$S_o + S_w = 1 \qquad (3\text{-}9)$$

$$\sum_x \omega_o^x = 1 \qquad (3\text{-}10)$$

$$\sum_x \omega_w^x = 1 \qquad (3\text{-}11)$$

$$k_{rw} + k_{ro} \leq 1 \qquad (3\text{-}12)$$

3.3 MASS TRANSFER

In the past, for the sake of mathematical simplicity, the pores were usually represented by cylindrical tubes. To describe the mass transfer process the pores are represented by straight triangular tubes. The size of the interface is the dominating factor for the mass transfer. Two distinct situations are considered in order to describe the mass transfer process. This approach is not continuous. Further, it needs to be mentioned that in this approach the mass transfer is dominated by the size of the interface between the water and the oil phase.

The first situation is valid for the situation where the radius of an oil blob in the triangular pore is smaller than the inscribed radius of the triangular pores (low oil saturations). The second situation is valid for the case where the blob radius is larger than the inscribed radius (high oil saturation). These two approximations are used to describe the mass transfer between the aqueous and the oil phase for either low (3-13) or high (3-14) oil saturations. All the derivations of these formulas are given in appendix D.

The first situation is represented by straight narrow cylindrical tubes placed in triangular tubes (Figure 3-2). The narrow tubes represent the pores and are saturated by both oil and water blobs. An error is made when the blob radius equals the inscribed radius of the triangle because the interaction area will be situated outside the inscribed circle of the triangle.

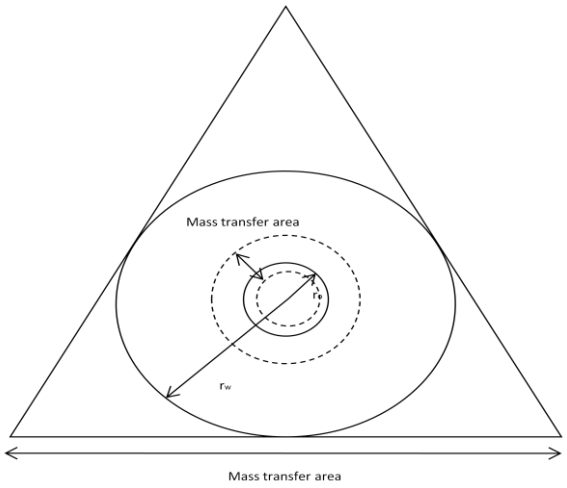

Figure 3-2: Model #1 for modeling mass transfer in triangular tubes (low saturations)

When the saturation increases so the blob radius exceeds the radius of the inscribed circle, a different approach is used resulting in a discontinuity in the mass transfer description. The interface through which mass transfer occurs is now described by the interface described by the three small triangles in the corners of the triangle (Figure 3-3) . Thereby, it is assumed that the interface between the oil and the water is a straight line. Also here the two-liquid film approach is used to describe the mass transfer. The dashed lines indicate the width over which the driving force is described.

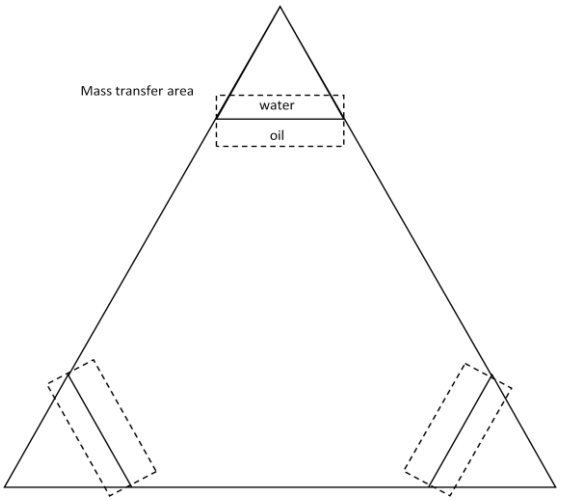

Figure 3-3: Model #2 for modeling mass transfer in triangular tubes (high saturations)

$$U = \frac{D^*}{1+S_o^{-1/2}}\left(k\cdot\rho_o\omega_o^{co_2}-\rho_w\omega_w^{co_2}\right),\ S_w<\frac{2}{\pi} \qquad (3\text{-}13)$$

$$U = D\left(\frac{3l_{side}}{4(A_{pore}S_w)}+\frac{l_{sidepore}}{4A_{pore}}\right)\frac{3l_{side}\phi}{A_{pore}}\left(k\cdot\rho_o\omega_o^{co_2}-\rho_w\omega_w^{co_2}\right),\ S_w>S_w<\frac{2}{\pi} \qquad (3\text{-}14)$$

4. NUMERICAL SIMULATIONS

In this chapter a simulator of a CWF process is presented. The simulator solves the equations using the Implicit Pressure Explicit Saturation (IMPES) method. The IMPES method is a fast approach on a time step basis, but it can have stability problems (Watts, 1986). The numerical model is based on a simulator developed by Valiollahi in 2005. It was developed to simulate the injection of oil-soluble chemicals in reservoirs (Valiollahi, 2005), incorporating reactive mass transfer in a two-phase flow system. For an accurate transformation, formulations have been added or adapted to suit the CWF process.

The numerical discretization is discussed first, together with numerical dispersion and the workflow of the model. Next, the approach for the sensitivity analyses is presented. Below is a table with all simulations executed in this work.

Simulation type	Parameters	Notes
Numerical Dispersion (7 simulations)	Grid block	Varying between 2 and 20 grid block
Numerical Dispersion (5 simulations)	Time Step	Varying between 0.1 and 1 [s]
Numerical Dispersion (3 simulations)	Standard water flood	Can show the impact of the number of grid blocks on numerical dispersion
Sensitivity (8 simulations)	Injection rate	An injection rate varying from 0.1 to 2 [ml min^{-1}]
Sensitivity (10 simulations)	Maximum solubility	Varying from 0 to 3 times the maximum solubility calculated with (2-2)
Sensitivity (6 simulations)	Pressure	Varying from 0.25 to 1.75 times the reservoir pressure
Sensitivity (6 simulations)	Residual oil function	Varying residual oil functions (Figure 2-6)
Sensitivity (7 simulations)	Diffusion constant	Varying between 10E-10 to 10E-13 [m^2s^{-1}]
Sensitivity (11 simulations)	Oil density	Varying from -1 to 2 times the density function (2-7)
Base case	All mechanisms	All mechanisms are chosen so that the simulator mimics the experiment as accurate as possible. Values are given in appendix E
Interfacial tension (2 simulations)	Residual oil function	One simulation where the residual oil saturation is not affected by the oil composition. Another simulation where it is the case

Table 4-1: All simulations performed in this study

4.1 DISCRETIZATION

The reservoir has been divided into *n* grid blocks. Every grid block contains specific information of every parameter at every time step. In addition to these *n* grid blocks an extra grid block *n+1* is added to the model to minimize the end effects. A schematic representation of the model is illustrated in Figure 4-1. In the simulation all values for every grid block are calculated every time step until the end time of the simulation is reached.(see also Figure 4-2).

Figure 4-1: Schematic representation of the model divided into grid blocks

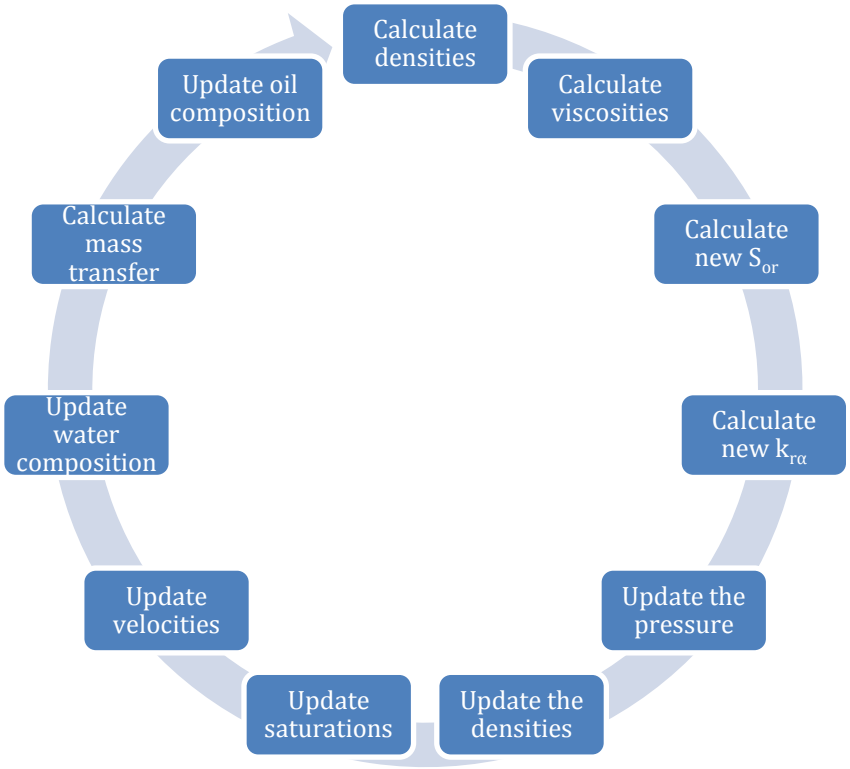

Figure 4-2: Step by step flowchart of the simulation for one time step

An effect of numerical discretization is numerical dispersion, which arises from time and space discretization that lead to smeared spatial gradients of saturation or composition. This results in saturation fronts that look like physical dispersion. Consequently, the water front that does not exhibit the same piston like displacement as shown by the analytical Buckley Leverett calculation. Three standard water flooding simulations have been run to illustrate this (see Figure 4-3). Here the number of grid blocks describing the reservoir is varied. Numerical dispersion occurs but is acceptable for 10 grid blocks and a time step of 0.5 seconds.

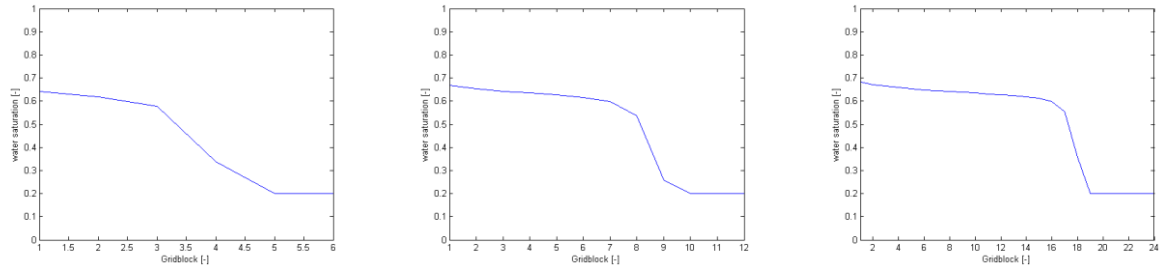

Figure 4-3: Buckley Leverett piston-like displacement computed with the simulator for 3 different cases. The numerical dispersion is largest in the left figure, which represent a waterfront in a 4 grid block simulation. The numerical dispersion decreases with the figures on the left which represent respectively 10 and 20 grid blocks.

4.2 Sensitivity Analyses

Sensitivity analyses are performed to investigate the influence of the different parameters on oil recovery by CWF and to validate the underlying mechanisms. A sensitivity analysis is a way to study how the variation of the output of a mathematical model can be apportioned to different sources of variation in the input. Simply, it is a technique to determine the influence on the output by changing the input.

The influence of oil swelling, viscosity reduction and a reduction of the residual oil saturation on the total oil production were studied as well as the influence of other parameters on these important physical aspects of CWF. The parameters that have been varied are the injection rate, maximum solubility of CO_2 in oil, pressure, residual oil function, diffusion coefficient, oil density and oil viscosity. The sensitivity analyses are performed on these parameters because they might influence the mass transfer (diffusion constant), the mobility of the oil (viscosity, residual oil saturation) the pressure in the system (injection rate, pressure), oil swelling (density) or define the limit of the mass transfer (maximum solubility of CO_2 in oil).

The sensitivity analysis is performed by introducing a weighing parameter α describing these paramters in the numerical model. A parameter is varied by changing the value of alpha (see also equations (4-1) tp (4-7)). To study the influence of this parameter, the other parameters are kept constant. The change in the results as a function of change in α is given in figures.

The oil swelling and the cumulative oil production cannot be directly varied in the simulation. However, the influence of the oil swelling can be deduced from the changing the other parameters.One of the results from the simulator is the total volume of oil produced and total volume of oil present in the core. These volumes are gathered from all simulation data and plotted versus the total volume of oil produced.

$$q_{inj,\alpha} = \alpha \cdot q_{inj} \quad (4\text{-}1)$$

$$sol_{\max,\alpha} = \alpha \cdot sol_{\max} \quad (4\text{-}2)$$

$$p_{\alpha} = \alpha \cdot p \quad (4\text{-}3)$$

$$S_{or,\alpha} = S_{or,init} \cdot \left[\omega_o^{CO_2} \right]^{\alpha} \quad (4\text{-}4)$$

$$D_{\alpha} = \alpha \cdot D \quad (4\text{-}5)$$

$$\rho_o = \alpha \cdot 21.826 \cdot \omega_o^{CO_2} + 773.19 \quad (4\text{-}6)$$

$$\log \mu = \omega_o^{'co_2} \log \mu_o^{co_2} + \omega_o^{'o} \log \mu_o^{o} + \alpha \omega_o^{'co_2} \omega_o^{'o} \quad (4\text{-}7)$$

5. EXPERIMENT

This chapter presents the experimental details. First the materials will be discussed, followed by the set-up. Then the procedure of the experiment with the data processing will be presented.

5.1 MATERIAL

The experiments are carried out using n-hexadecane as model oil at ambient temperature and pressures up to 25 bar. The water in the model is water with 20.000 ppm dissolved NaCl, also called brine. The gas is CO_2, supplied by LINDE with a purity of 99.7%. The most important properties of n-hexadecane, brine and CO_2 are described in the table below.

Property	Value	Unit
Molecular formula hexadecane	$C_{16}H_{34}$	[-]
Molar mass hexadecane	226.44	[gr mol^{-1}]
Density hexadecane	773	[kg m^{-3}]
Density brine	1015.40	[kg m^{-3}]
Maximum solubility of CO_2 in brine at 25 bar (mass fraction) (Diamond, et al., 2002)	0.0371	[-]

Table 5-1: Properties of the fluids used in the experiments

The experiments were carried out with a Bentheimer sandstone core. The length of the core is 17 centimeters with a radius of 1.4 centimeter. The porosity measurements have been performed with the Ultrapycnometer 1000. Repeating this measurement 10 times results in an average porosity of 0.26. The permeability measurements are determined with a Ruska wet (liquid permeameter). The resulting permeability of this measurement is 1.2 Darcy. The details of these porosity and permeability measurements are given in appendix B and summarized in Table 5-2.

Other core characteristics have been determined by flooding the core with pure water followed by pure hexadecane. This is carried out by mimicking nature's way of oil migration and production into an oil reservoir, until the core is residual oil saturated. Accompanying these steps is the knowledge of dead volume and Pore Volume (PV), connate water saturation S_{wc} and residual oil saturation S_{or}. These core characteristics can also be used in the numerical model. In Table 5-3 the steps and the results thereof are shown. In appendix B.3 and B.4 the details of these steps can be found.

Parameter	Value	Unit
Porosity (Ultrapycnometer)	0.26	[-]
Permeability (Ruska wet permeameter)	1.2	[Darcy]
Dead volume	30.12	[ml]
Pore Volume	40.68	[ml]
S_{wc}	0.20	[-]
S_{or}	0.27	[-]

OIIP	24.74	[gr]
Residual oil after water flooding	8.35	[gr]

Table 5-2: Characteristics of the core used for the CWF experiment.

Step #	Action	Result	Value	Unit
1	Measure the volume of the complete set-up except for the core	Dead volume	30.12	[ml]
2	Saturate core with brine	Pore volume	40.68	[ml]
3	Imbibition until no more water is being produced	S_{wc}	0.20	[-]
4	Drainage until no more oil is being produced	S_{or}	0.27	[-]

Table 5-3: Steps undertaken to determine core characteristics

5.2 Experimental Set-Up

Figure 5-1 shows schematically the experimental set-up used to conduct the experiments. The set-up is described in detail in appendix B. It consists of:

- Pressurized vessel (1a – 1c);
  - Pressurized vessel (1a);
  - Pressure meter (1b);
  - CO_2 tank (1c);
- Backpressure valve (2a – 2b);
  - Backpressure valve (2a);
  - Nitrogen tank (2b);
- Pump (3);
- High pressure density meter (4);
- Core (5);
- Outflow collector (6a – 6c);
  - 50 ml burette (6a);
  - scale (6b);
  - wet gas meter (6c);
- Switches (s).

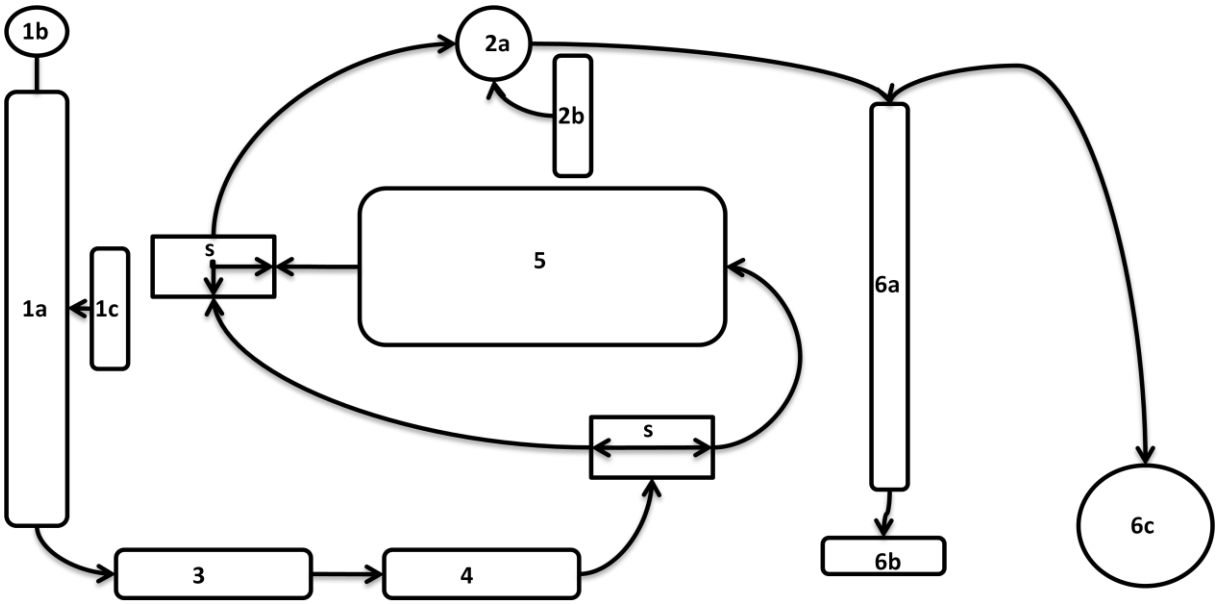

Figure 5-1: The schematic representation of the experiment

Figure 5-2: Photo of the experimental set-up

5.3 PROCEDURE

5.3.1 EXPERIMENT

For the CWF experiment water saturated with CO2 is injected into a core at residual oil saturation. The injection rate is 1 cm^3 min^{-1} at ambient temperature and a pressure of 25 bar. This corresponds to a field flow rate of 1 m day^{-1}. The injection of carbonated water was interrupted after 8 hours and recommences at 24 hours. This 24 hour sequence is repeated for 5 days. The experiment can therefore be summarized as the repetition of two periods, 8 hours of injection, 8 hours 'soaking'.

Period	Time	Notes
1	0 – 8 hours	Injection of carbonated water
2	8 – 24 hours	No injection
3	24 – 32 hours	Injection of carbonated water

Table 5-4: First three periods of the experiment

The volumes of water and oil present in the outflow collector (burette) are measured every 10 minutes. Every 30 minutes the produced liquid phases are sampled separately from the burette and weighed. The samples are then evacuated to ensure no more CO2 is dissolved.

5.3.2 DATA PROCESSING

From the data of CWF experiments production profiles for oil, gas and water as a function of injected Pore Volumes (PV) and time are constructed. Two sets of data results from the CWF experiments. The first set of data from the inlet are:

- The injected volume of carbonated water;
- The pressure of the carbonated water;
- The density of the carbonated water.

At the outlet production data is gathered:

- The produced mass and volume of the pure water phase;
- The produced mass and volume of the pure oil phase;
- The produced volume of the CO_2 (if no CO_2 is still in solution in the produced oil and water phase).

6. RESULTS & DISCUSSION

In this chapter the results of the simulations and the experiment are presented and discussed. First the results of the numerical analyses are discussed. This is followed by the results of the experiments. Then the numerical results will be validated with the experimental data. This verification is accompanied by the investigation to all mechanisms in the CWF process.

6.1 SIMULATIONS

6.1.1 GRID BLOCK SIZE AND TIME STEP

First, the sensitivity of the results of the model on the grid block size and on the time step was investigated. Therefore, the fractional flow of oil (2-12) has been computed. If the fractional flow of oil increases linearly over the length of the core at each time it can be assumed that the model can be linearized. This means that the number of grid blocks does not have large impact on the results of the model. The model has been run with a high number of grid blocks (50) and a small time step (0.1 second).

Figure 6-1 shows that the fractional flow curves of oil as function of the distance at various simulation times of 2.5, 5, 7.5 and 10 hours. These graphs show that the fractional flow of oil actually can be assumed to increase linearly with distance, in particular for times longer than 5 hours. The results for 5 hours show a small bump. The cause of the bump is unknown but might indicate an oil bank being displaced in the porous medium like discussed in the work of De Nevers (1966). For times below this 5 hours the fractional flow is not linear. However, the value of the fractional flow of oil is so small that without introducing a too large error it can be assumed linear as well. In Figure 6-2 the influence of the number of grid blocks and the time step on the cumulative oil production is shown. The cumulative oil production does not change in the range of chosen time steps and for more than 10 grid blocks.

The time step size is empirically optimized. As seen in Figure 6-2, the time step (in the chosen range) does not influence the resulting total amount of produced oil . In Figure 6-3 is shown that if the time step is chosen too long, and thus the simulation time is shortened, the results show artifacts, e.g. a discontinuity in the oil fraction. These artifacts seem to be a result of the boundary conditions.

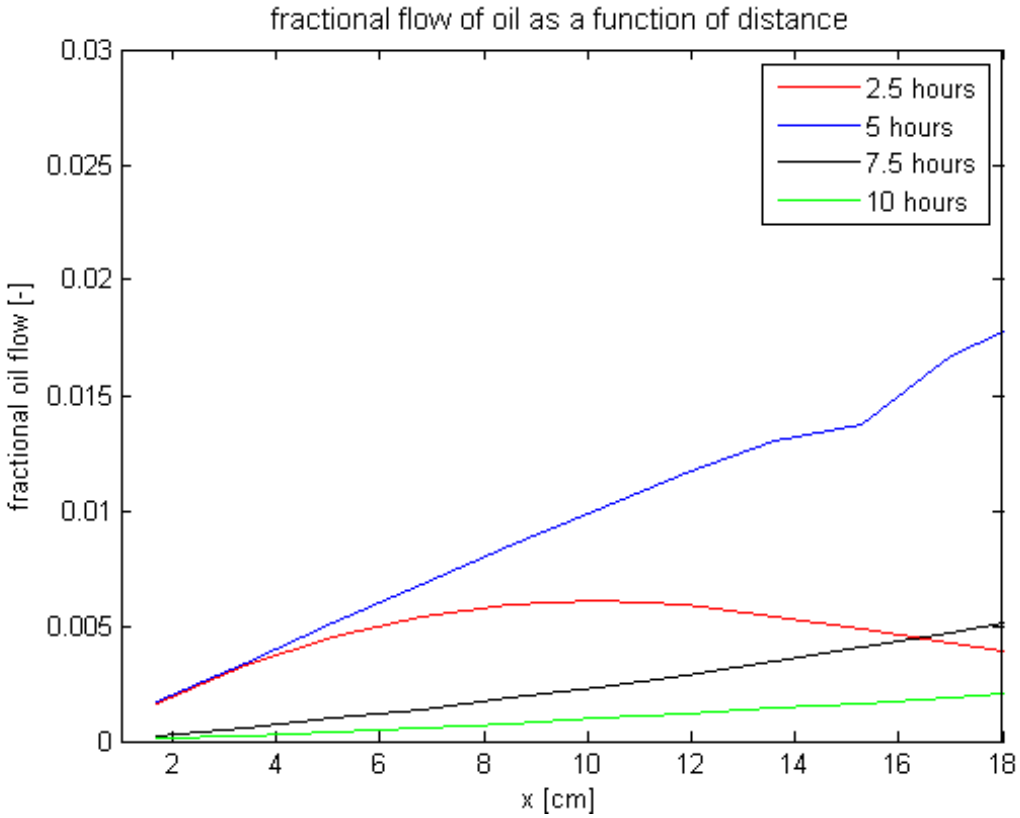

Figure 6-1: Fractional flow of oil as a function of distance at several times in the simulation

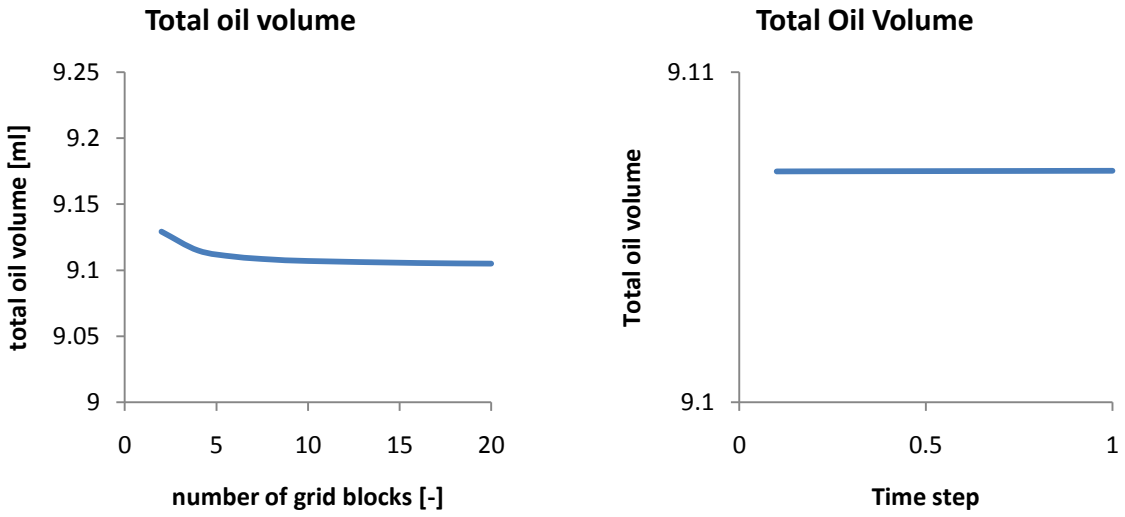

Figure 6-2: Cumulative produced oil volume after 10 hours of simulation as function of the number of grid blocks used for discretization (left). Total volume of oil after 10 hours of simulation to show the influence of the time step (right)

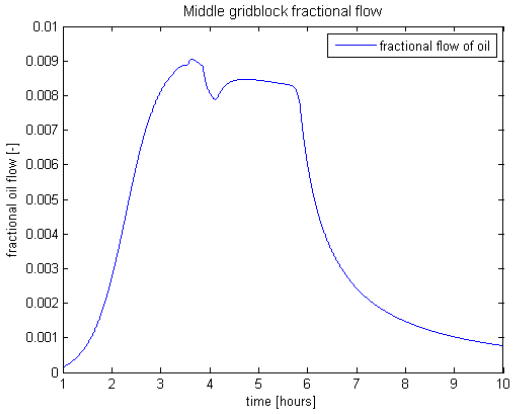

Figure 6-3: An artifact appears in the results of the residual oil

6.2 SIMULATION

The results of the simulation show that oil production commences after 3 hours of injecting carbonated water (see Figure 6-4). This equals a volume of injected carbonated water of 4 PV. The cumulative oil production increases quickly up to 15 hours (22.5 PV) of injection before it stabilizes. The constant value of the cumulative oil production implies that all mobile oil is displaced. The cause of the oil production increase between 4 and 22.5 PV's might be either the reduced residual oil saturation or an oil bank as discussed in De Nevers (1966), or both. However, the formation of an oil bank should be indicated by an increase in the fraction flow of oil. Only a small increase in the fractional flow of oil is observed for simulation times of 2.5 hours and 5 hours but not for longer times (see Figure 6-1).

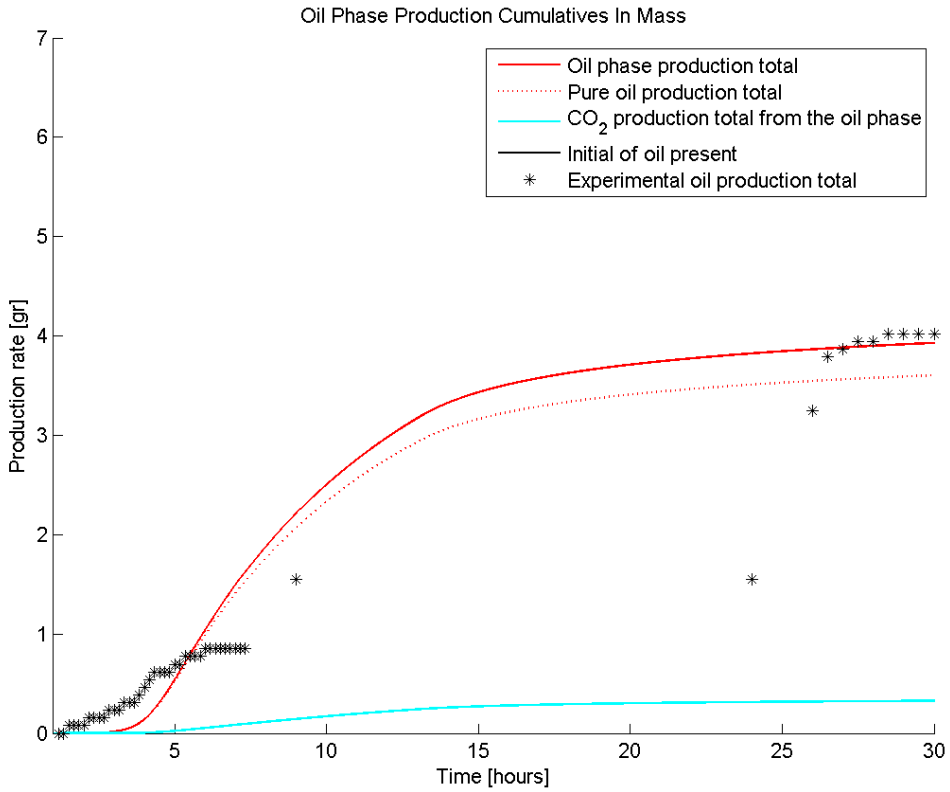

Figure 6-4: Production profile where IFT affects the CWF process

6.3 VALIDATION OF THE SIMULATOR WITH THE EXPERIMENT

6.3.1 EXPERIMENT

In total three experiments have been carried out. The first two experiments were performed to optimize the set-up.

For the last experiment carbonated water was injected with a rate of 1 cm^3 min^{-1} for 250 hours with periods of 8 hours of no injection (paragraph 5.3.1).

Even though carbonated water was injected for 250 hours, significant oil production only occurred in the first 30 hours of the experimental run. Therefore, only the oil production as function of time is shown for 30 hours. The total oil production as a function of injected PV is given up to 20 PV (Figure 6-5).

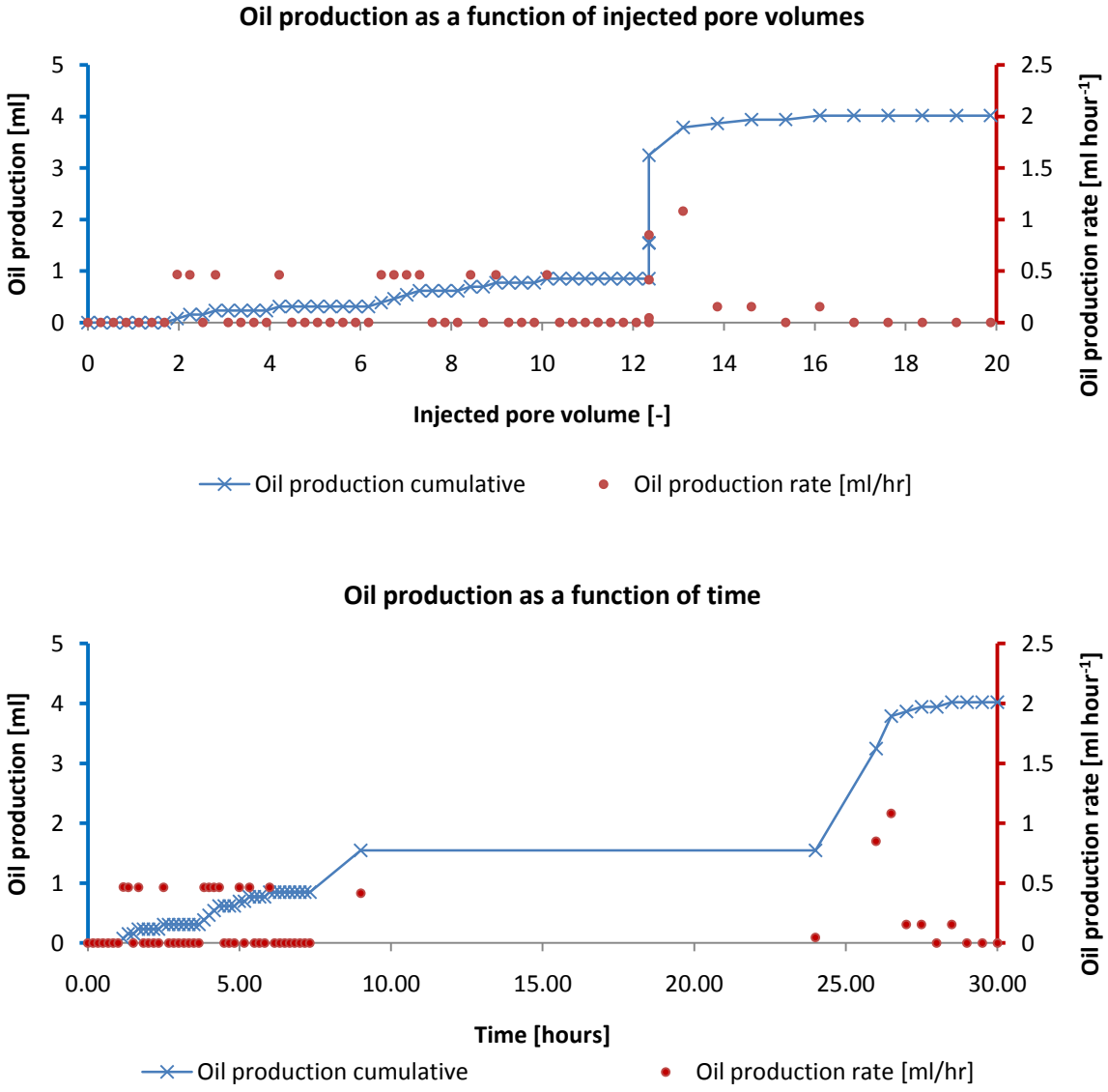

Figure 6-5: Oil production cumulative and rate as a function of injected pore volume (top) and time (bottom). The produced fluids are at ambient temperature and pressure

The oil production as a function of time can be divided into three main parts as displayed in Table 5-4. In the first period (up to 8 hours) only a relatively small amount of the OIIP is produced. In the second period, between 8 and 24 hours, no more carbonated water is injected but still some oil is produced. In the third period the production increases sharply for 3 hours before it stabilizes. Apparently, the oil production rate can reach a higher value after the soaking period than before the soaking period. This is also visible in the top graph in Figure 6-5, where a sharp increase in oil production is seen around 12 PV of carbonated water injected. It is not clear if this increase of the oil production after the stagnation of the oil production when no carbonated water was injected, is due to the soaking or if it is 'just' the continuation of the oil production if water was continuously injected. If 'soaking' would be the reason for the increase of the oil production, then the diffusion of CO2 from the water phase into the oil phase would

determine the oil production. If it would be the continuation of the oil production, it would indicate that an oil bank reached the outlet.

In Figure 6-6 the cumulative produced CO_2 and water is displayed as function of time at ambient pressure and temperature. The cumulative water production shows the same trends as oil. The cumulative CO_2 production increases continuously, though the increase in CO_2 production is stronger in the times when carbonated water is injected. In particular, the cumulative production of CO2 supports the hypothesis that oil banking occurs and that the oil production is actually the same as if continuously carbonated water is injected.

The total amount of hexadecane produced at the end of the experiment is 4.02 gram of the 8.60 gram hexadecane present at the initial situation. After 250 hours in total, 4.79 gram hexadecane was produced. The Oil In Place (OIP) after applying CWF is 3.81 gram. This is an ultimate recovery of 83.35% of the OIIP, which is about 20% higher than the ultimate recovery of a water flood which is 62.41%. The final residual oil saturation is 0.128.

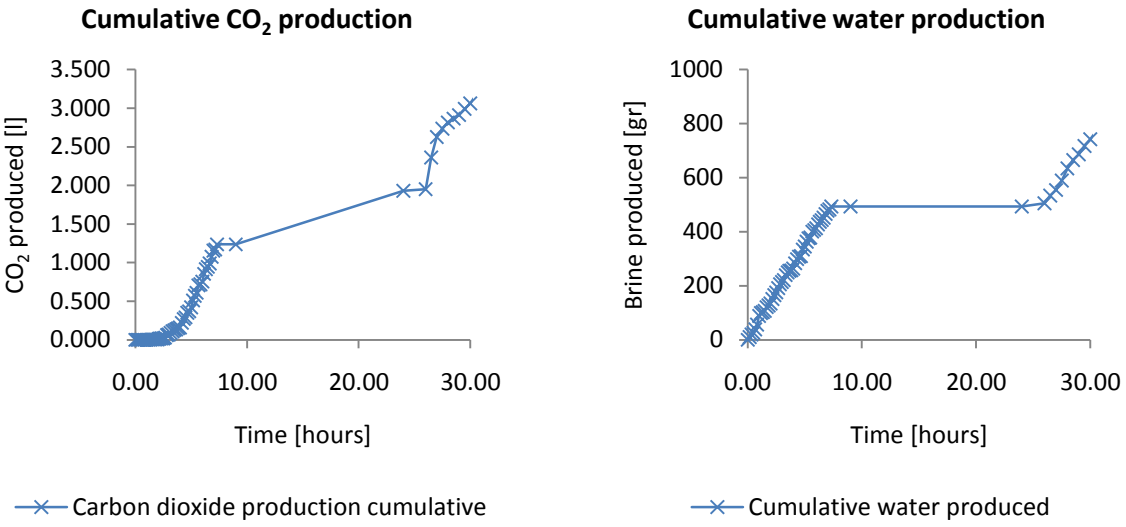

Figure 6-6: Cumulative CO_2 and water production at ambient temperature and pressure

In the burette which was used to collect and separate the water, oil and CO_2 produced, a white scale was observed on the interface between the aqueous and the oil phase (Figure 6-7). This precipitation of some unknown component on the interface is a result of CO_2 transferring from the brine into the oil phase. Unfortunately, the amount of precipitate was too small to perform a chemical analysis.

Figure 6-7: Picture of the white scale in the outlet collector

6.3.2 Comparison of the Experimental Data with Simulation Results

In Figure 6-8 the comparison of experimental determined oil production and the simulated oil production as function of time is given. The input parameters and assumptions are given in appendix E. In the simulation, the injection rate was set to zero for a rime period between 8 and 24 hours to match the experimental data.

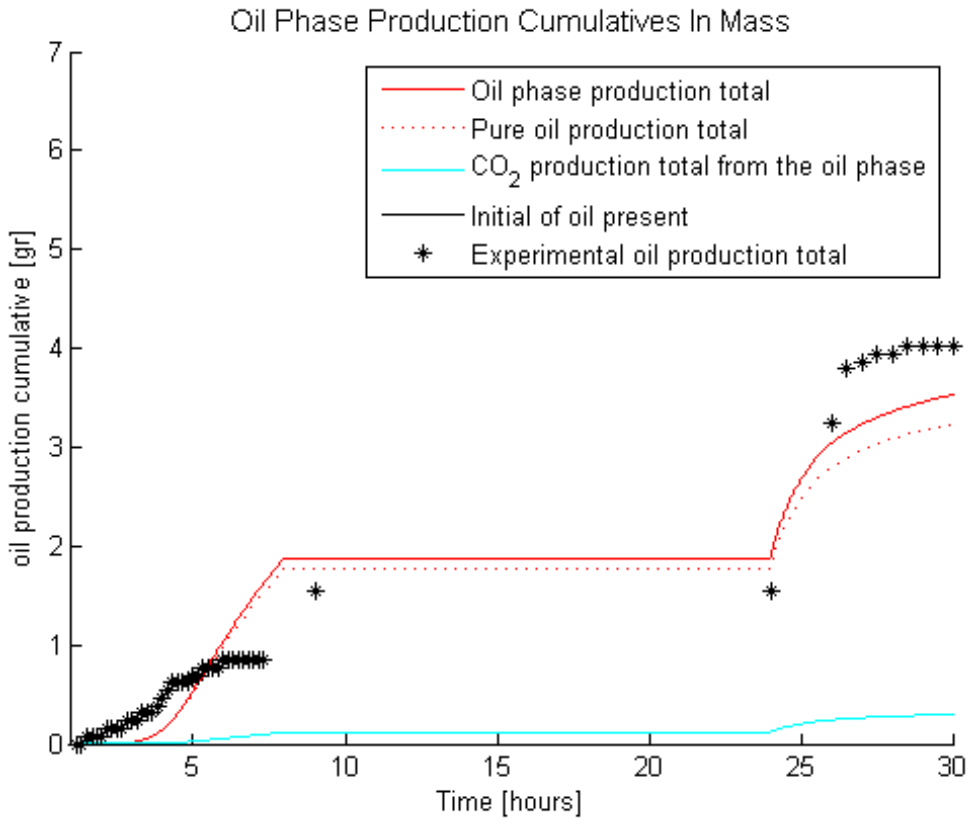

Figure 6-8: Comparison of experimental data and a numerical model. The cumulative oil production is plotted as function of time

In general, the simulation could reproduce the experimental data, although the final oil volume recovered is not the same. It must be mentioned however, that in order to accomplish similar results as the experiment some values had to be estimated. For example, the correction factor (distribution coefficient) in equation (2–1) was adjusted to get a better fit. The best fit was found for a distribution coefficient of 0.35. The distribution coefficient is defined as the ratio of the mole fractions of CO2 dissolved in the water phase and of the mole fractions of dissolved CO2 in the oil phase. Thus a value of 0.35 sounds realistic as the solubility of CO_2 in water is smaller than in the oil phase. Additionally, the diffusion coefficient was lowered by factor 10 to a 100. Such an decrease in the diffusion coefficient of CO2 means that diffusion crucial for the describing the carbonated water flood.

6.4 MECHANISMS OF THE CWF PROCESS

In Figure 6-9 the computed cumulative mass transfer and the mass transfer rate of CO_2 from the aqueous phase to the oil phase is given. In particular in the initial period the mass transfer increases to a high rate before it drops gradually. The initial strong increase might be explained by the increase of interfacial area between the oil and the water at the beginning of the injection of carbonated water. The decrease of the rate of mass transfer after around 1.5 hours shows that still more CO_2 is transferred from the aqueous phase into the oil phase as continuously carbonated water is injected. Less CO_2 is transferred as the driving force for mass transfer decreases; the concentration of CO_2 in the oil phases approaches its equilibrium concentration. After the injection of carbonated water has stopped, the rate of mass transfer decreases slightly stronger before it almost becomes zero after around 20 hours. Only after the injection of carbonated water has started again, a slight increase in CO_2 mass transfer is observed (around 24 hours). A possible explanation might be that due to the injection the interfacial area is increased. However, after 1 ½ hours the mass transfer rate has become zero again. This indicates that the oil phase has reached CO_2 saturation. From this analysis, it can be concluded that the mass transfer of CO2 from the aqueous into the oil phase is mainly at the beginning of the process and the for longer times, the mass transfer plays a minor role as the oil phase reached its saturation. Nevertheless, it is interesting to note, that after the injection of carbonated water has stopped, mass transfer of CO_2 from the aqueous phase into the oil phase continues changing the properties of the oil slightly.

In Figure 6-14 the CO_2 mass fractions in the oil and the aqueous phase as function of time are shown for the grid block in the center of the core. This figure illustrates the CO_2 mass transfer from the aqueous into the oil phase. The mass fractions of CO_2 in the water phase first increases strongly until it reaches the composition of the injected carbonated water. Due to the continuous injection of carbonated water, the mass fractions of CO_2 in the aqueous phase stays constant. After 8 hours the injection of carbonated water stops and a slight decrease of CO_2 mass fractions in the aqueous phase is observed. After injection of carbonated water commences at around 24 hours, the mass fractions of CO_2 in the aqueous phase increases immediately up to the composition of the injected carbonated water. Analyzing the change of composition of the oil phase; here it can be seen that the mass fractions of CO_2 into the oil phase increases continuously until around 15 hours. This shows that indeed the mass transfer of CO2 into the oil

phase continues even though injection of carbonated water has stopped after 8 hours. After injection of carbonated water is started again (at around 24 hours), a further increase in the mass fractions CO_2 in the oil phase is observed before it the composition of the oil phase is constant. The final ratio of mass fractions of CO_2 in the aqueous and oil phase is according to the applied distribution factor describing the distribution of CO2 over the water and oil phase at equilibrium (see equation 2-10 with $k = x_{co2}^{o} / x_{co2}^{aq}$). Thus after around 25 hours no additional CO2 is transferred from the aqueous into the oil phase because the concentrations of CO2 in the oil phase has reached its maximum value.

Figure 6-11 illustrates the variation of the (residual) oil and water saturation with time. Both figures represent the behavior in the grid block in the center of the core. Initially, the water saturation decreases. This behavior is quite striking as already in this period oil production has started so that it would have been expected that the water saturation increased while the oil saturation decreased. The saturations shown in this graph are at the center of the core. Therefore, it might be possible that this increase in oil saturation is the indication of the formation of an oil bank. Though, another possible explanation for this behavior is that the water saturation decreases due to an increase in density. At the same time, oil production has started. Therefore, the increase in water density and thus a decrease of the water saturation in the core is compensated partially by the decrease of the oil saturation due to oil production. After around 4 hours the water has reached its minimum density and the water saturation increases again. This increase continues until injection of carbonated water is ceased (around 8 hours). Then a slight decrease of water saturation with at the same time a slight increase of the residual oil saturation. This is due to the mass transfer of CO_2 from the aqueous phase into the oil phase and the accompanied density and composition changes. When injection of carbonated water starts again (around 24 hours), the water saturation up to its final value of 0.8

In the first period, an increase in the oil saturation is observed and almost no oil is produced; this is thus the effect of oil swelling. A slight oil swelling is also observed in the second period during which no carbonated water was injected. This is also illustrated in Figure 6-12, which shows the volume of both the oil present in the core, the oil produced as well as the sum thereof. The sum is constant throughout the simulation time if no oil swelling occurs. If an increase is observed, oil swelling occurred. When the injection starts, the total oil volume rises to a volume which is about 15% higher than the initial oil volume. During the second phase the oil swells only slightly. Remarkable is that the final total volume of oil in the core is high (more than the starting volume minus the produced oil). This is clearly an indication that CO_2 has been transported from the aqueous phase into the oil phase.

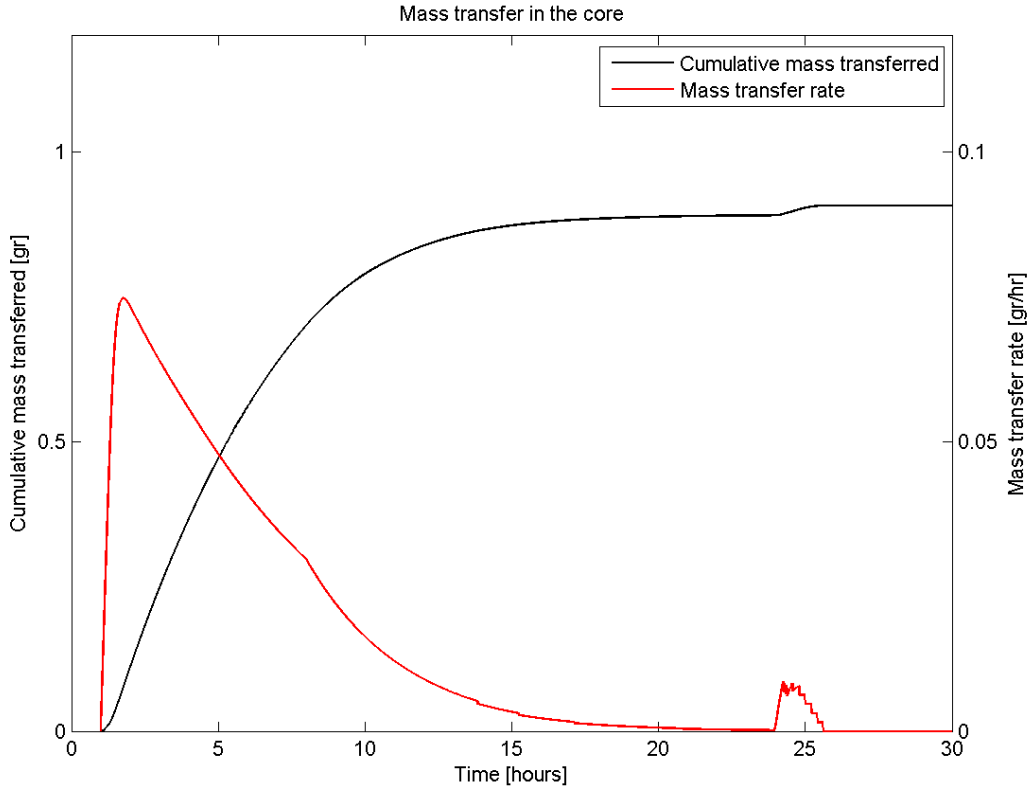

Figure 6-9: Mass transfer of CO_2 from the aqueous phase into the oil phase as a function of time

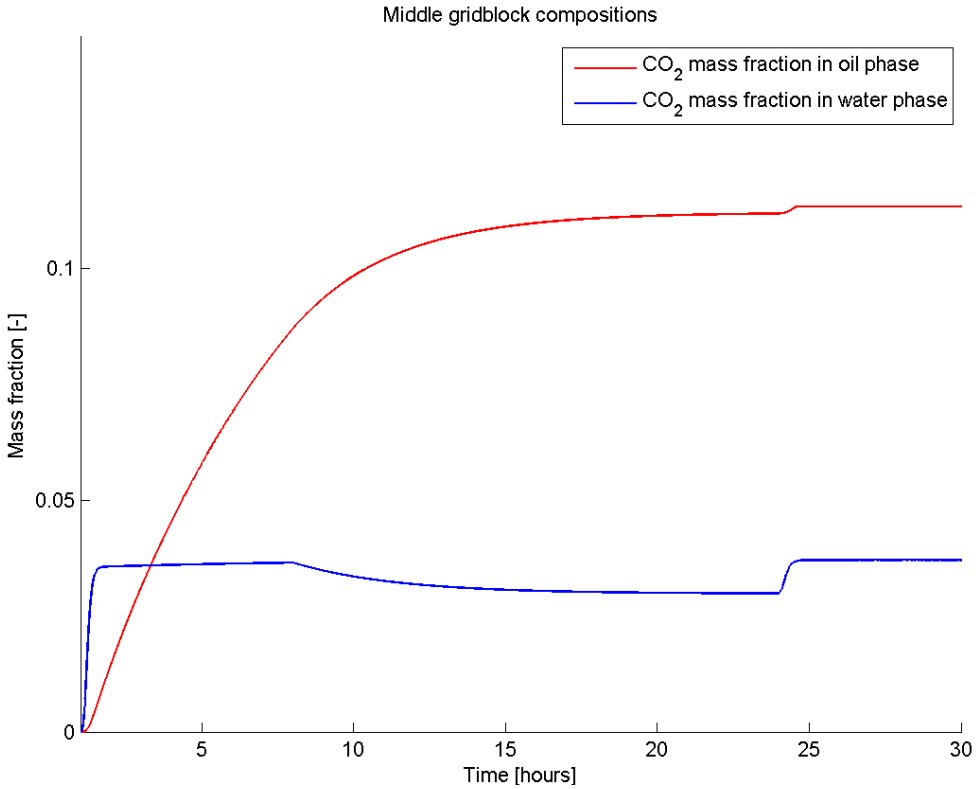

Figure 6-10: CO_2 fractions in the oil and water phase as a function of time

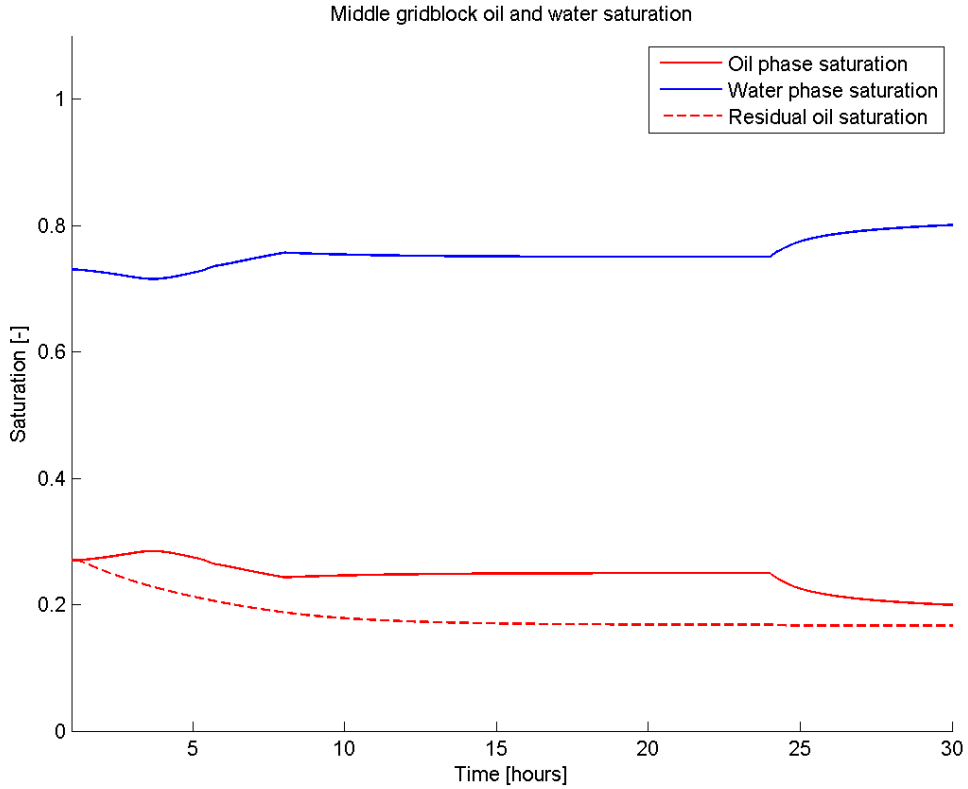

Figure 6-11: Saturation of the center grid block as a function of time

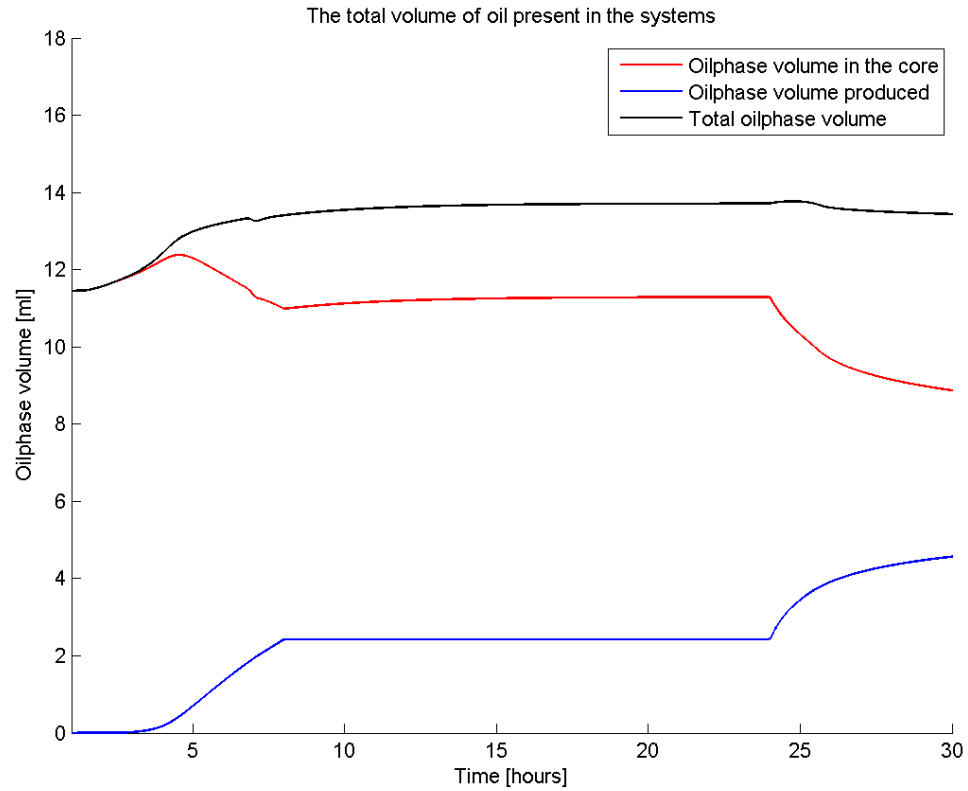

Figure 6-12: Oil volume present in the simulation

6.5 RESIDUAL OIL SATURATION FUNCTION

Another simulation was to show the influence of the residual oil function in the simulator. For this simulation a continuous injection rate of 1 cm^3 min^{-1} is computed. The resulting cumulative oil production as function of time, assuming a constant residual oil saturation is shown in Figure 6-13. It can be observed that in the case where the residual oil does not change with composition, the total production is close to 1 gram of hexadecane compared to 4.02 in the experimental data, which is added in the same figure. The exact same case where residual oil is affected constant shows a total oil production of about 4 gram (Figure 6-14), which equals the experimental data (added to the figure). If it is assumed that the residual oil saturation is independent of the composition, less CO_2 is produced together with the oil. Additionally, oil production commences much later if the IFT is assumed to be constant.

Figure 6-15 shows the saturation profiles for the case that the residual oil saturation is constant, Figure 6-16 for the case where the residual oil saturation changes with composition. In the model where the residual oil saturation is not affected by the composition of the oil the residual oil saturation remains constant. The oil saturation rises slightly but the amount of mobile oil does not increase significantly. In Figure 6-16 it can be seen that for a composition dependent residual oil saturation, the amount of mobile oil is much larger.

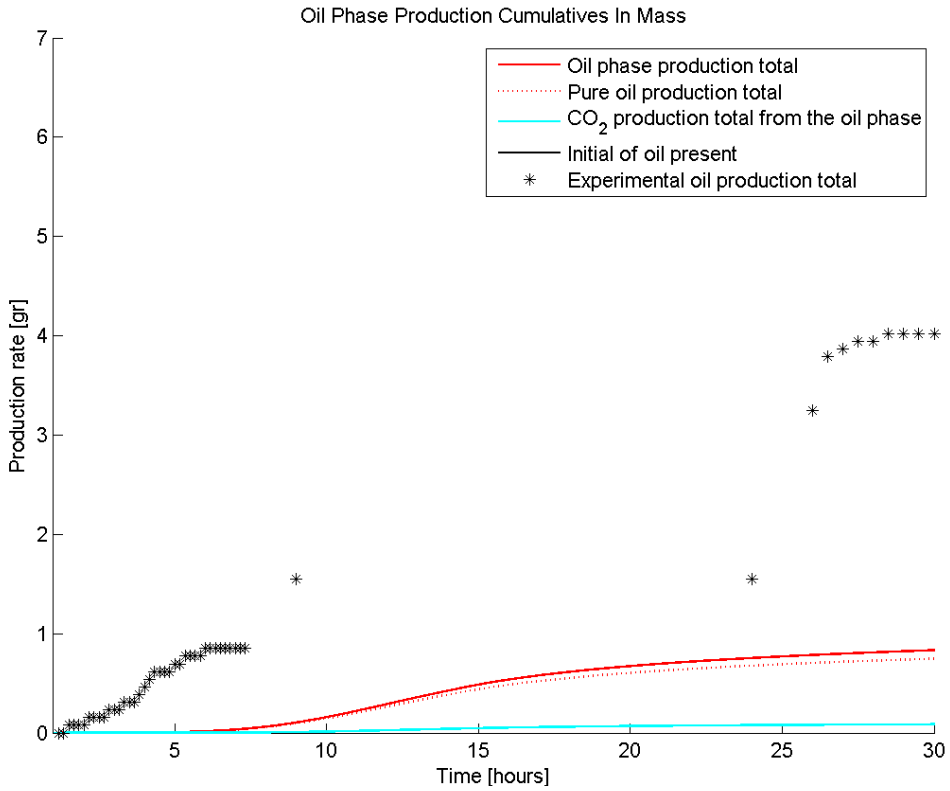

Figure 6-13: Production profile where IFT does not affect the CWF process

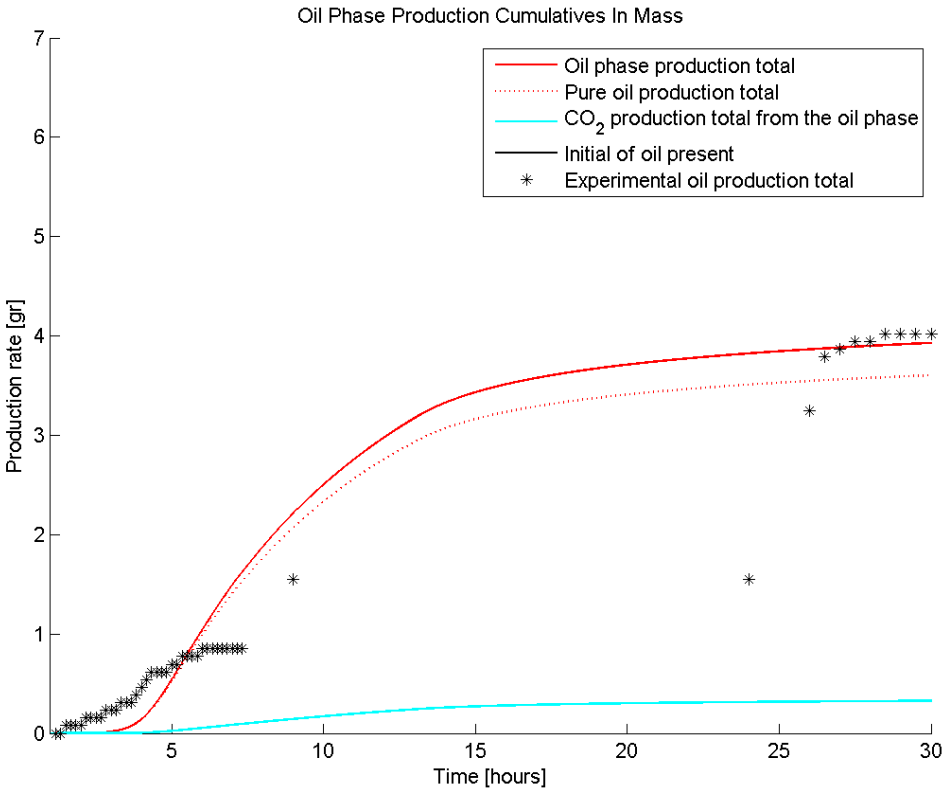

Figure 6-14: Production profile where IFT affects the CWF process

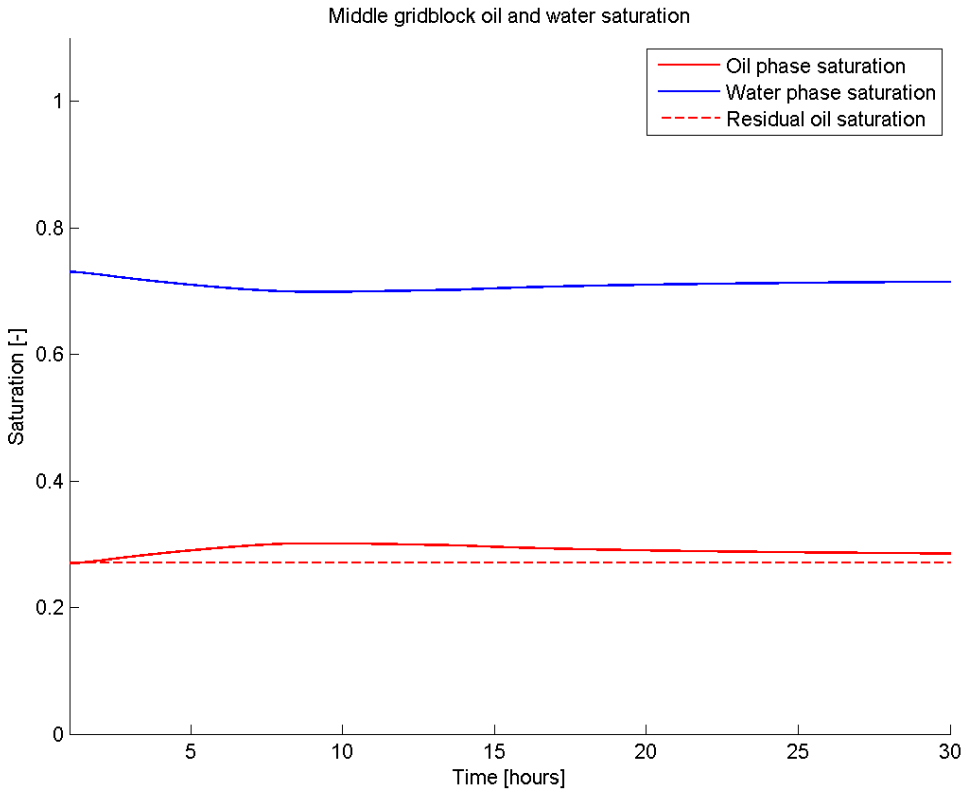

Figure 6-15: Saturation profiles of the case where IFT does not affect the system

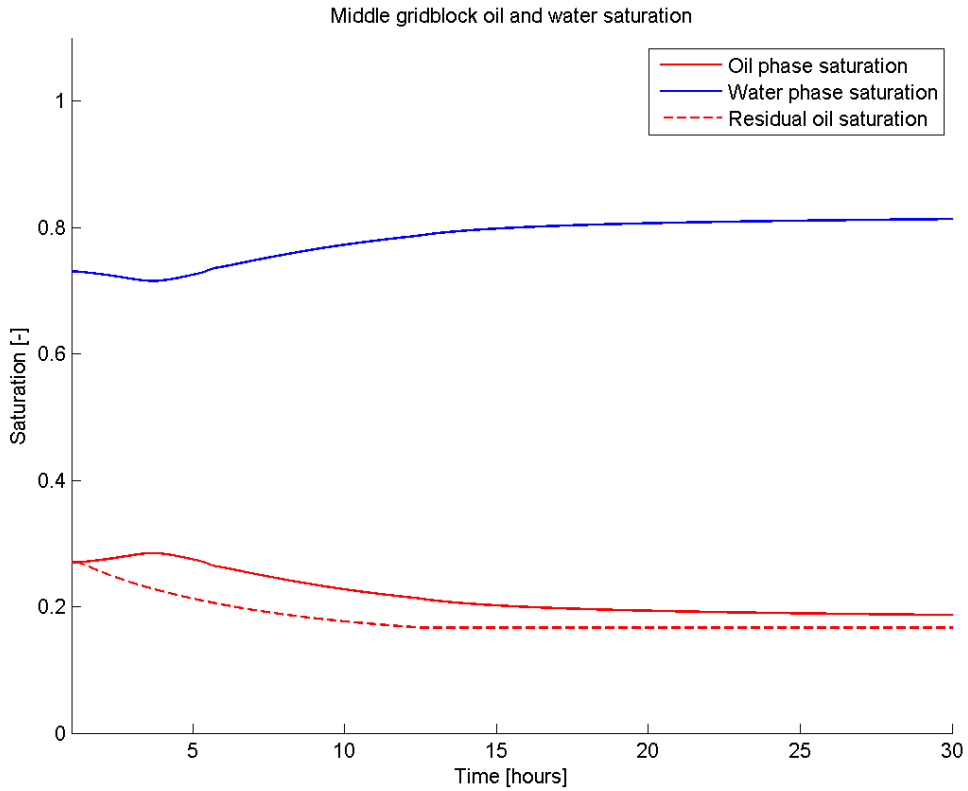

Figure 6-16: Saturation profiles of the case where IFT affects the system

6.6 Sensitivity Analysis

For this sensitivity study 48 simulations have been run for which the injection rate, the maximum solubility, pressure, diffusion coefficient, residual oil saturation, oil viscosity and density have been varied. In Figure 6-17 to Figure 6-20 the so-called spider plots are given in which it is depicted how the cumulative oil production, after 5 and 30 hours, the oil swelling and the viscosity are affected by changes of these properties. In Figure 6-21 the correlation between oil swelling and improved oil production is shown.

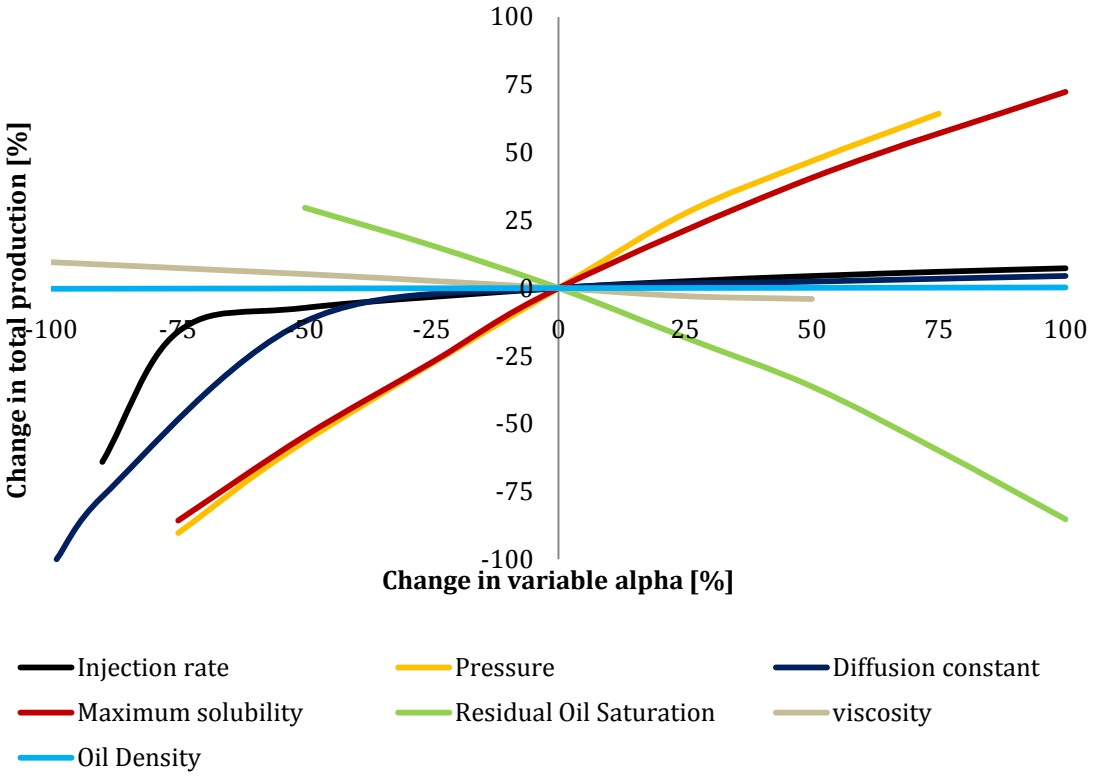

Figure 6-17: Sensitivity analysis on total production after 30 hours of simulation

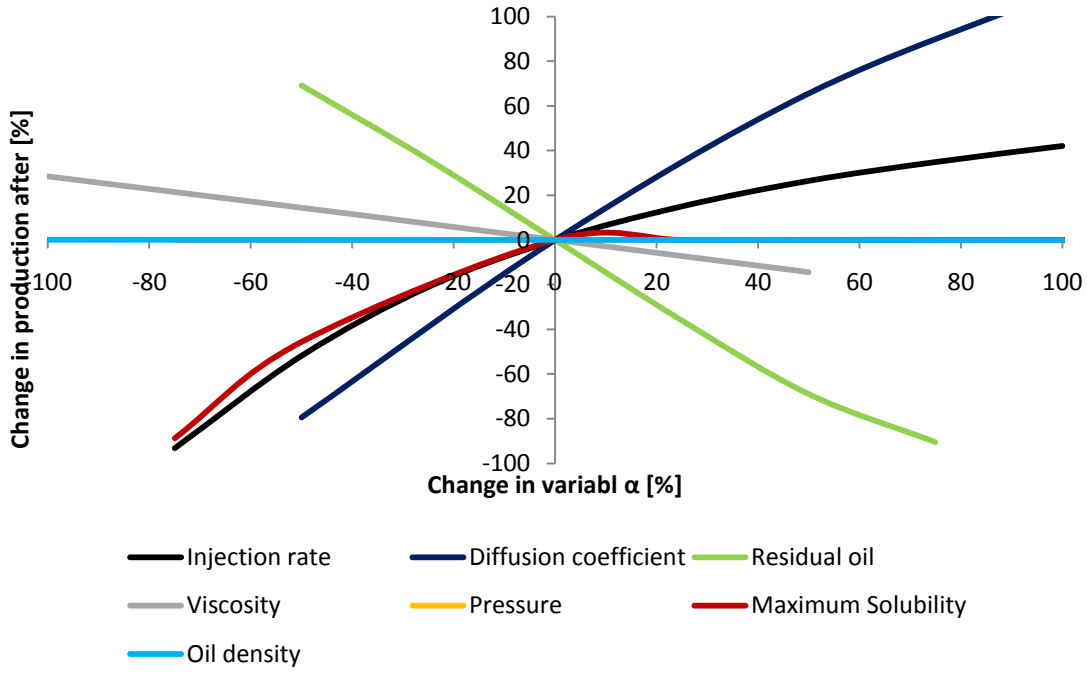

Figure 6-18: Sensitivity analysis on the speed of the process, by plotting the total production after 5 hours of simulation

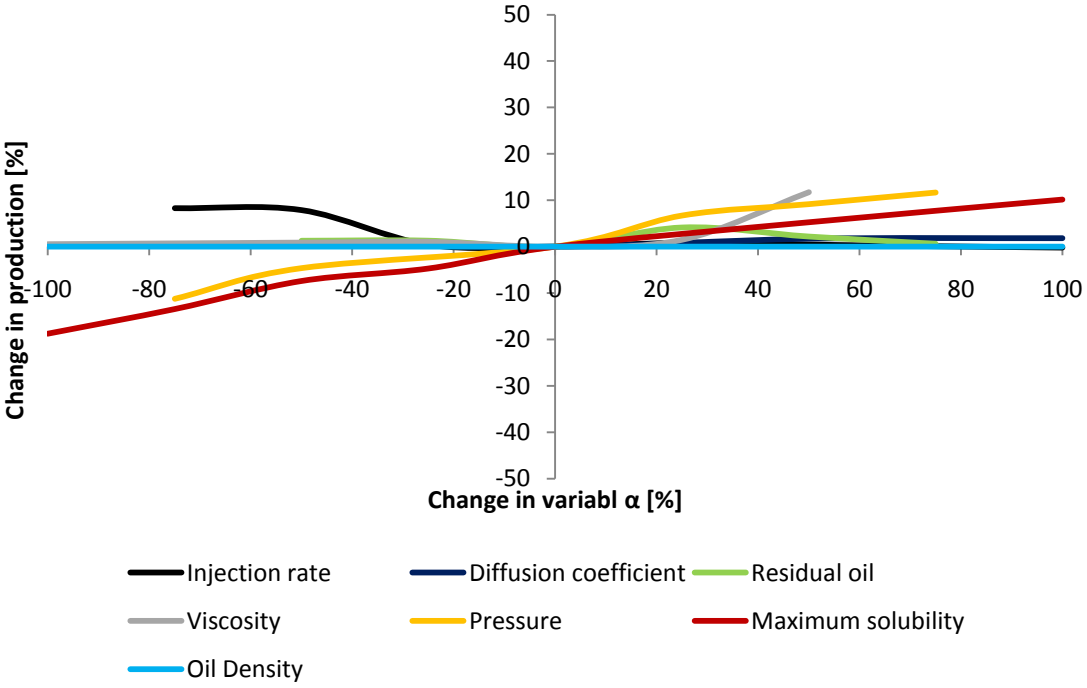

Figure 6-19: Sensitivity analysis on the oil swelling after 30 hours of simulation

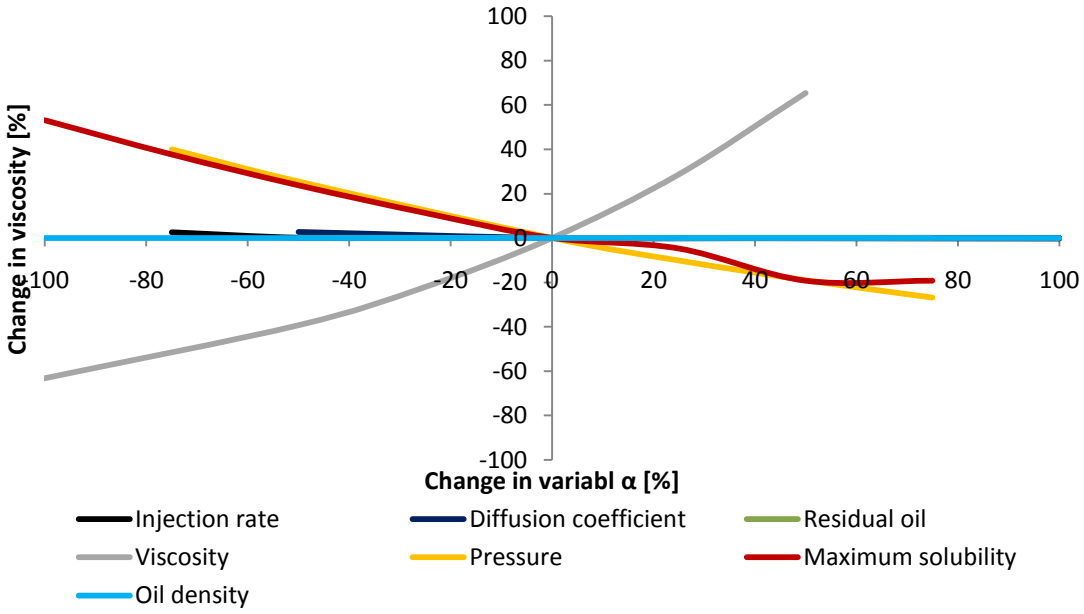

Figure 6-20: Sensitivity analysis on the influence of viscosity after 30 hours of simulation

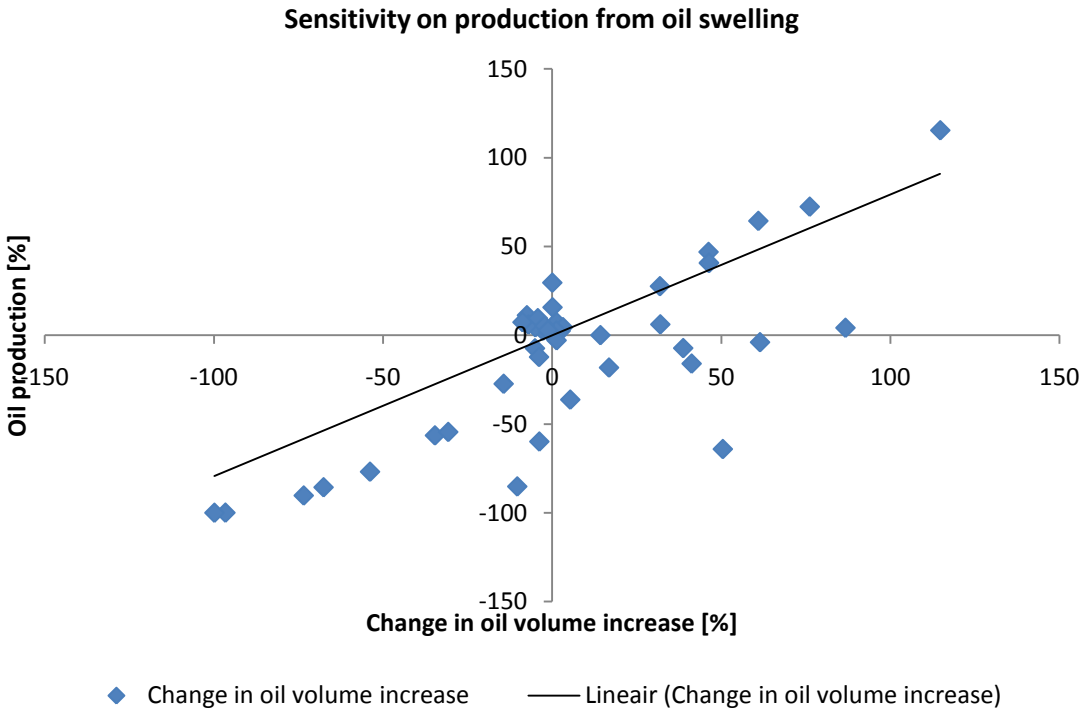

Figure 6-21: Sensitivity analysis on the influence of oil swelling

From Figure 6-17 and Figure 6-18 it can be concluded that the effect on the total oil production by changing one of the parameters is less if the simulation is run for a longer period (30 hours instead of 5 hours). Interestingly, the simulation is sensitive to variations of all parameters if the simulation time is 5 hours. For a simulation of time of 30 hours, only the pressure, maximum

solubility and the residual oil saturation, indirectly the changes in IFT have a strong effect on the resulting cumulative oil production. Changes in the oil density have barely influence on the cumulative production, the viscosity has only a slight influence. The injection rate and diffusion constant show some influence. However, comparing the results after 5 hours of simulation and 30 hours of simulations, it can be concluded that the viscosity and diffusion constant have no influence if the production/simulation time is further increased. Comparing the two figures, it can be seen that in particular the diffusion coefficient has a strong influence. For short simulation times, decreasing and increasing D changes the cumulative oil production while for simulation times of 30 hours, there is mainly variation in the cumulative oil production if the coefficient is decreased. This indicates that the speed of the mass transfer has strong influence on the success of injecting carbonated water. Therefore it is important to know the right value for this constant. For too low diffusion constant values the process might become mass transfer dependent, which is not the expected result.

The variation in oil swelling due to changes of the other parameters is less pronounced than for the cumulative oil production (Figure 6-19). The most influence is seen for the injection rate, pressure and maximum solubility. The influence of the pressure and the maximum solubility is straight forward because these properties actually determine almost directly the degree of oil swelling. The influence of the injection rate is not as straight forward. The smaller the injection rate, the more the oil swells. This means that for lower injection rates at the given diffusion coefficient more CO_2 transfer from the aqueous phase to the oil phase. The effect of decreasing the injection rate is not seen in the variation of the viscosity Figure 6-20. The viscosity only clearly changes upon changes of the pressure and the maximum solubility.

A final study was performed to identify the influence of oil swelling on the total oil production (Figure 6-21). As expected the cumulative oil production increases with increasing oil swelling. The increase in oil production is almost directly proportional to the oil swelling.

6.7 DISCUSSION

The experiments performed were still preliminary and need some adjustment to allow a quantitative analysis of the process. A necessary modification is the dead volume of the set-up. This is rather large compared to the pore volume, since the ratio is 30 ml to 40 ml. Therefore, a small error in the determination of the dead volume can result in significant errors in the determination of pore volume, connate water and residual oil saturation. These values are then used as input parameters for the simulations which then might result in inaccurate results. Further, the determination of the outflow needs to be improved.

Another uncertainty in the experiment arises when determining the core characteristics. In the process, the injected fluid changes from water to oil to carbonated water. Every time the injected fluid changes several milliliters of fluid are lost at either the inlet of the outlet. This is due to the pressure in the system that is being released. It is also common that a small leak will occur during any time in the experiment. This will also result in wrong estimates for total volumes.

Another necessary improvement of the experiment would be to make it a continuous injection process. The shortcoming of this investigation is to prove if oil banking occurs, which is probably the case due to the 'creation' of mobile oil. This oil bank is not really visible in the experiment because the soaking period leaves too much room for other causes of the increased production. The increased oil production in the third is probably an oil bank. The simulator does not show this oil bank because the grid blocks are probably chosen too small.

In the set-up facilities were included to study the density of the water entering the core and determining the volume of CO_2 produced at the outlet. Due to mechanical defects the density has not been measured. The volume of CO_2 produced has been recorded but not studied in depth, due to lack of time. The produced fluids were produced continuously, but measured at fixed moments which might cause errors, as well as the fact that CO_2 might still be present in the produced fluids.

Nevers (1964), Simon and Graue (1965), Emera and Sarma (2006), Al-Quraini et al (2007), Enayati et al (2008) all focus on oil swelling and viscosity reduction in oil-CO_2 flooding processes. They present these effects as main reasons to produce additional oil from reservoirs. Although it is shown in the simulator that these indeed have an effect on oil production, the increased oil production is not enough to mimic the experiment. The error in this process is either due to measurement errors in the experiment or numerical errors in the simulator, or due to the fact that the residual oil saturation might be reduced as a consequence of dissolved CO_2 in the organic phase. Another option might be the distribution coefficient of 0.35 and the maximum solubility of CO_2 in hexadecane which limit the process.

The comparison with the Buckley Leverett analysis of De Nevers (1964) is hard to accomplish. Since oil banking has not been noticed in the investigation it is hard to strengthen or disprove the research already done. Therefore additional experiments must be performed under continuous injection. However, it must be noted that CWF consists of three phases, which occur at almost the same time since the speed of the mass transfer is very large:

1. Transport of the CO_2 into the reservoir;
2. Mass transfer of the CO_2 from the water phase to the oil phase;
3. Displacing the swollen oil in an environment where the residual oil saturation might have decreased.

7. CONCLUSIONS AND RECOMMENDATIONS

7.1 INTRODUCTION

From the results and discussion in previous chapter 5.3.2, conclusions can be drawn with respect to the objectives stated in chapter 1. In addition to the conclusions, several recommendations are given to improve this research or for future research.

7.2 CONCLUSIONS

- A simulator is designed and built in MATLAB. The resulting changes in the characteristics of the fluids due to the composition change and both mass transfer from the carbonated water into the oil and from the oil into the water was accounted for. The model has been validated with the experimental data;
- The simulations show that the additional oil recovery is affected by the oil swelling and the reduction of residual oil saturation. The reduced residual oil saturation implies indirectly a reduced interfacial tension. The reduction in viscosity is a factor that affects mostly the speed of the process. An increased volume of oil accounts almost for the same increase in production. The reduced residual oil saturation accounts for the majority of the increased oil production;
- An experiment was designed and built to execute a CWF experiment. The method of CWF clearly results in incremental oil recovery under given conditions. With the experiment an ultimate recovery of 83%, compared to 62% for water flooding. The final residual oil saturation is 12.8;
- The increased oil production in the experiment is probably due to an oil bank reaching the outlet. However, this cannot be proven with the experiment as carried out in this investigation;
- The maximum solubility of CO_2 in the oil and water phase is the limiting factor in the CWF process. Sensitivity analyses show that the maximum solubility drives the change in oil swelling, viscosity reduction and reduction of residual oil saturation. Pressure has a direct influence on this maximum solubility;
- Oil swelling alone will not account for enough incremental oil recovery. This is either due to errors in the experiment or simulation or due the reduced residual oil saturation which is affected by a reduced interfacial tension.

7.3 RECOMMENDATIONS

- Design the set-up of the experiment in such a way that it does not have to be disconnected;
- Use a core with a much higher pore volume, this way the ratio between the pore volume and the dead volume will improve the differentiating capabilities of the experiment;
- Determine a strategy to define exactly the concentration of CO_2 in the injected carbonated water;

- Improve the outflow collector so more characteristics of the produced fluids can be determined;
- Perform a CWF experiment with continuous injection to show oil banking;
- Design experiment to investigate solely the PVT behavior of the system, this could be:
    - Volume of oil as a function of CO_2 content under different pressures;
    - Maximum solubility of CO_2 in hexadecane;
    - IFT between oil and water for different compositions of oil-CO_2 and water-CO_2.
- When completed all these elementary researches, try expanding this study by including CT scanner in the set-up so the process while CWF can be monitored more precise;
- A better way of solving the numerical system is by using a Jacobian. It makes the whole numerical system implicit and therefore produces a smaller error;
- Expand the model with a gravity term to analyze the sweep of this method;
- Include the reaction of CO_2 with water which makes the water a weak acid. This is expected to create a higher injectivity in reservoirs (Nevers, 1964).
- Expand the study to real heavy oils, possibly combined with a thermal method.

8. REFERENCES

Al-Jarba M. and Al-Anazi B.D. A Comparison Study of the CO2-Oil Physical Properties Literature Correlations Accuracy Using Visual Basic Modelling Technique [Journal]. - [s.l.] : Oil and Gas Business, 2009.

Al-Quraini A., Sohrabi M and Jamiolahmady M Heavy Oil Recovery by liquid CO2/water Injection [Journal] // Society of Petroleum Engineers. - 2007.

Cinar Y., Marquez S. and Orr Jr. F.M. Effect of IFT Variation and Wettability on Three-Phase Relative Permeability [Journal] // SPE Reservoir Evaluation & Engineering, Volume 10, Number 3. - 2007. - pp. pp. 211-220.

CO2 global [Online] // http://www.co2.no.

DeRuiter R.A., Nash L.J. and Singletary M.S. Solubility and displacement Behavior of a Viscous Crude With CO2 and Hydrocarbon Gases [Journal]. - [s.l.] : SPE, 1994. - Vol. May.

Diamond L.W. and Akinfiev N.N. Solubility of CO2 in water from - 1.5 to 100 C and from 0.1 to 100 MPa: evaluation of literature data and thermodynamic modelling [Journal]. - Bern : Elsevier, 2002.

do Pereira Siqueira Campos C.E. [et al.] Solubility of Carbon Dioxide in Water and Hexadecane: Experimental Measurement and Thermodynamic Modeling [Journal]. - [s.l.] : Journal of Chemical Engineering Data, 2009. - 10 : Vol. 54.

Emera M.K. and Sarma H.K. A Genetic Algorithm-Based Model to predict CO2-Oil physical Properties for Dead and Live Oil [Journal]. - [s.l.] : Petroleum Society, 2006. - Vol. 197.

Enayati M and Heidaryan E New Investigations into Carbon Dioxide Flooding by Focusing on Viscosity and Swelling Factor Changes [Journal]. - [s.l.] : Petroleum Society, 2008. - Vol. 64.

Grunberg L. and Nissan A.H. Nature, 164:799 [Book]. - 1949.

Hebach A, Oberhof A and Dahmen N Density of water + carbon dioxide at elevated pressures: measurements and correlation [Journal]. - [s.l.] : Journal of Chemical Engineering Data, 2004. - 4 : Vol. 49.

Helland J.O. and Skjaeveland S.M. Physically based capillary pressure correlation for mixed-wet reservoirs from a bundle of tubes model [Book]. - 2006.

Heriot Watt Institute of PetroleumEngineering http://www.pet.hw.ac.uk [Online]. - 08 26, 2010. - 2010.

Kobayashi R, Charoensombut-Amon T and Martin R.J. Application of a generalized multiproperty apparatus to measure phase equilibrium and vapor phase densities of supercritical carbon dioxide in n-hexadecane systems up to 26 MPa [Journal]. - [s.l.] : Eslevier Science Publishers, 1986. - Vol. 31.

Nevers De A Calculation Method for Carbonated Water Flooding [Book]. - 1964.

Riazi M [et al.] Oil Recovery Improvement Using CO2 - enriched water injection [Journal] // Society of Petroleum Engineers. - 2009.

Simon R and Graue D.J. Generalized Correlations for Predicting Solubility, Swelling and Viscosity behavior of CO2-Crude Oil Systems [Journal]. - [s.l.] : Journal of Petroleum Technology, 1965. - Vol. January.

Srivastava R.K. [et al.] Measurement and Prediction of PVT Properties of Heavy and Medium Oils With Carbon Dioxide [Journal]. - 1995.

Tran T.S. and Zitha P. L. J. Electromagnetic Assisted Carbonated Water Flooding for Heavy Oil Recovery [Conference] // World Heavy Oil Congress. - [s.l.] : WHOC, 2009.

Treybal R.E. Mass-Transfer operations [Book]. - [s.l.] : McGraw-Hill, 1980.

Valiollahi Modeling of the Placement of an Oil-Soluble Chemical in Porous Media for Water Control [Book]. - Delft : Delft University of Technology, 2005.

Watts J.W. A Compositional Formulation of the Pressure and Saturation Equations [Journal]. - [s.l.] : SPE, 1986. - Volume 1, number 3 : Vol. 1986.

Wesselingh J.A. and Krishna R. Mass Transfer [Book]. - 1990.

Whitson C. and Brule M. Phase Behavior [Journal]. - [s.l.] : SPE, 2000. - Vol. 20.

A. APPENDIX ON MATERIAL AND SET-UP

Property	Value	Unit
Molecular formula	$C_{16}H_{34}$	[-]
Molar mass	226.44	[gr/mol]
Melting point	291	[K]
Boiling point	560	[K]
Specific gravity	0.77	[-]
Solubility	Insoluble in water	[-]

Table A-1: n-Hexadecane properties

Criteria	Condition
T_c = 304.19 K	Temperature below which no miscibility will take place
P_c = 73.80 bar	Pressure below which no miscibility will take place

Table A-2: CO_2 properties

Substance	Density	Unit
Density brine	1015.40	[gr/l]
Maximum solubility of CO_2 at 25 bar (mass fraction)	0.0371	[-]

Table A-3: water properties

The set-up of the experiment consists of:

- Pressurized vessel (1a – 1c): The pressurized vessel (1a) will be used to dissolve CO_2 into the injection water. In order to inject a constant portion of CO_2 into the water, the pressure will be kept constant. This pressure is constantly monitored at pressure meter 1b. This is done by constantly increasing the amount of CO_2 in the vessel from a CO_2 tank (1c) when water is being injected into the core. A constant pressure of 25 bar will result in a constant solubility of CO_2 in the water. The volume of the vessel is 500 ml.
- Backpressure valve (2a – 2b): The backpressure valve (2a) aims on keeping a constant pressure of 25 bar at the outlet. This pressure is applied by piling up the pressure with a nitrogen tank (2b). Together with the injection rate this controls the pressure system in the core.
- Pump (3): The pump can be adjusted to a certain injection rate of 1 milliliter per minute. The injection increases the pressure at the inlet of the core above the 25 bar of the backpressure valve. Now a driving force is created which makes the flow of brine and oil possible.
- CO_2 content measuring (4): Right after the pump a device will be installed to measure if the CO_2 content is as calculated. This will be determined with a high pressure density meter. This measures the density of the fluid passing through. This can be used to define the amount of CO_2 in solution.

- Core (5): In the set-up the core will be placed horizontally. This is due to the presence of CO_2 which might have an additional effect due to gravitational forces. The core is residual oil saturated after water flooding.
- Outflow collector (6): The outflow of the core will be collected in a 50 ml burette (6a) attached to a wet gas meter (6c). This way, the amount of gas that comes out of solution can be measured as well as the amount of oil and water. The burette is above a scale (6b) which can measure the total weight of water and oil produced.
- Two points are included in the set-up which can alter the flowpath. These are two three-way switches which can direct the flow so it can include or bypass the core. The bypassing path is used for determining the dead volume without dismantling any part of the set-up.

B. APPENDIX ON EXPERIMENTAL DATA

This chapter describes all experimental actions prior to the core flooding. First the porosity and permeability measurements are described, followed by the experiments to determine the core characteristics.

B.1 POROSITY

The porosity measurement will be performed with the Ultrapycnometer 1000. This device measures the matrix volume and the true density of the present sample. With the matrix volume and the volume of the sample the void space, or the porosity, can be calculated according to formula (B-1). In this formula 'φ' is the porosity. This is a function of the volume of the bulk matrix 'V_b' and the volume matrix 'V_{ma}'. This results in a porosity of 0.26.

$$\phi = \frac{V_b - V_{ma}}{V_b} \qquad \text{(B-1)}$$

Run	Volume [cm³]	Density [g cm-3]
1	11.4556	2.6895
2	11.4999	2.6792
3	11.5066	2.6776
4	11.5177	2.6750
5	11.5199	2.6745
6	11.5362	2.6707
7	11.5381	2.6703
8	11.5424	2.6693
9	11.5464	2.6684
10	11.5514	2.6672
Average	11.5214	2.6742

Table B-1: Ultrapycnometer results for calculating the porosity of the core

Parameter	Value	Unit
Mass	30.81	[g]
Temperature	26.30	[deg C]
Core length	30.00	[mm]
Diameter	25.70	[mm]
Radius	12.85	[mm]
Bulk volume	15.56	[cm³]

Table B-2: Core characteristics for calculating the porosity of the core

B.2 PERMEABILITY

The permeability measurements have been performed with a Ruska dry (gas) and wet (liquid) permeameter. The gas permeameter is an instrument developed for the measurement of the

permeability of a core, by directing a gas flow through it. The pressure drop over the core, the temperature of the gas and the measured flow through the core provide enough information to calculate the permeability with the help of formula (B-2). In this formula 'k' is the permeability. This is a function of viscosity of the gas 'μ_g', flow rate 'Q', length of the core 'L', the area of the cross-section of the core 'A' and the pressure drop over the core 'Δp'.

$$k = \frac{\mu_g q L}{A \Delta p} \qquad \text{(B-2)}$$

The disadvantage of this method is that gas slippage occurs. Gas slippage results in a higher apparent permeability. This can be corrected using the Klinkenberg formula. The klinkenberg permeability 'k_g' is shown in formula (B-3) and is a function of flow rate 'q', gas viscosity 'μ_g', injection pressure 'p_1', atmospheric pressure 'p_2', internal radius of tip seal 'a' and a geometric factor 'G'.

$$k_g = q \mu_g \frac{p_1}{a} G \left(p_1^2 - p_2^2 \right)^2 \qquad \text{(B-3)}$$

Calculating the permeability using the wet permeameter, the cores are first saturated with a fluid and weighed. The porosity can be calculated and the following formula can be applied. In this formula 't' is the time. The advantage of this method is that is does not need a correction. With the use of this method we obtained a permeability of 1.2 Darcy for the core.

$$k = \frac{\mu_g V L}{A \Delta p t} \qquad \text{(B-4)}$$

The results of the porosity and permeability experiments are calculated as in appendix 0. Also the final choice for permeability and porosity for the model is derived from this experiment and is shown in appendix E and Table 5-2.

For the permeability is chosen to use the Ruska wet permeameter because the permeability will not have to be corrected for gas slippage. In the following table the results of the measurements are shown.

Parameter	Value	Unit
Temperature	21.00	[deg C]
Core length	3.00	[cm]
Diameter	27.70	[mm]
Radius	12.85	[mm]
Area	5.1874	[cm^2]
Pressure drop	0.5	[atm]
Liquid viscosity	0.95	[cp]
Volume	50	[cm^3]
Time	46	[s]

Table B-3: Core characteristics for calculating the permeability of the core

With this input the result of formula (B-4) will be 1.2 Darcy.

B.3 DEAD VOLUME

This is the volume of all the parts of the set-up excluding the core. This is an important parameter to know since it is critical to know at any stage during the experiment how big the volumes of the fluids are and where they are located.

Before determining the dead volume we have dried the complete set-up by injecting CO_2. The determination of the dead volume is executed by injecting 20 gram per liter NaCl into the set-up (at point 3). The brine passes through the high pressure density (4) meter and bypasses the core (5). After the backpressure valve (2) the fluids are collected in the outflow collector (6). Brine will be injected until brine will be produced. As soon as the first drop of brine enters the outflow collector, the pump must stop injecting brine. Instead, the pump will now inject plain air to flood the brine through the system. When there is no more brine production in the outflow collector, the set-up will be dried again by injecting CO_2. This is to guarantee that there is no brine left in the set-up. The amount of volume now present in the outflow collector is the dead volume. To get good results this test must be repeated several times. We have performed this five times and the results are shown below in Table B-4.

Volume	Unit
26.34	ml
25.27	ml
31.21	ml
34.40	ml
35.36	ml

Table B-4: Results for determining the dead volume of the experimental set-up

This results in an average dead volume of 30.12 milliliter. This value will be used as volume not present in the core.

B.4 PV, CONNATE WATER SATURATION AND RESIDUAL OIL SATURATION

A crucial step in the preparation stage is to mimic nature's way of originating a reservoir. First the core will be saturated with brine. Next, oil will migrate into the 'reservoir', followed by an injection of brine to imitate the first two production stages of oil recovery. Additional core characteristics here are Pore Volume (PV), connate water saturation and residual oil saturation. The PV is the amount of void space in the core which is able to contain fluids. Connate water saturation is the lowest possible volume of water that cannot be produced from the core. Residual oil water saturation is the lowest possible volume of oil that cannot be produced with brine injection. Since these last parameters follow the injection of brine it is also called the residual oil saturation after brine or water flooding. The results are shown in Table B-5.

At first we saturated the core with brine. Another goal for this step is to derive the pore volume of the core. It also simulates nature's first step in the origination of a reservoir. The pore volume is the total amount of void space in the core (5). The switches (s) must now be adjusted so that the fluids will pass through the core. Also the backpressure valve (2) will now be installed to the

desired pressure of 25 bar. Brine will be injected by the pump (3) through all the parts of the set-up and collected in the outflow collector (6). This injection should continue until at least 10 pore volumes have been injected into the core. Since the pore volume is not known in front of this stage it is assumed that 500 milliliter will suffice. It will be calculated with the help of equation (B-5) which calculates the pore volume (PV) with the amount of brine that is injected '$V_{w,inj}$' and produced '$V_{w,prod}$' minus the dead volume 'V_{dead}'.

$$PV = V_{w,inj} - V_{w,prod} - V_{dead} \quad (B\text{-}5)$$

The second step is to flood oil into the core. This is also called imbibition. A core characteristic gathered from this stage is the connate water volume. Now hexadecane will be injected into the system. The pump (3) will inject the oil through the complete set-up and the outflow will be collected again (6). Again, at least 10 PV's must be injected to sufficiently saturate the core with hexadecane. Another way is to continue injecting oil until no more brine is being produced. Then it can be assumed that there is no brine left in the pipes of the set-up. With this step, the connate water saturation 'S_{wc}' can be calculated with the help of (B-6) and (B-7). First, the volume of water in the core '$V_{w,core}$' must be known.

$$V_{w,core} = PV - V_{dead} - V_{w,prod} \quad (B\text{-}6)$$

$$S_{wc} = \frac{V_{w,\,core}}{PV} \quad (B\text{-}7)$$

The final step in the preparation stage is to mimic the production stage of oil production, also called drainage. By injecting brine into the system until no more hexadecane is produced this can be determined. The brine drains all hexadecane out of the pipes and only a few hexadecane will be left in the core. This is the residual oil saturation after water flooding. With the help of formulas (B-8) and (B-9), the residual oil saturation 'S_{or}' can be calculated. Now the most important values of the core are known and the experiment is ready to commence. The results of the core characteristics can be seen in Table B-5 below.

$$V_{o,core} = PV - V_{dead} - V_{o,prod} \quad (B\text{-}8)$$

$$S_{or} = \frac{V_{o,\,core}}{PV} \quad (B\text{-}9)$$

Characteristic	Value	Unit
Dead volume	30.12	ml
Brine injected in phase 1	70.27	ml
Pore Volume	40.68	ml
Brine produced in phase 2	62.50	ml
$C_{16}H_{34}$ injected in phase 2	61.97	ml
S_{wc}	0.20	[-]
Brine injected in phase 3	64.98	ml
$C_{16}H_{34}$ produced in phase 3	48.56	ml
S_{or}	0.27	[-]

Table B-5: Summary of the determination of the core characteristics

C. APPENDIX ON THE NUMERICAL DISCRETIZATION OF THE MODEL

In order to solve the equation obtained in chapter 0, the following procedure is taken. To formulate and discretize the oil pressure and saturation parameters, the IMPES method is chosen. In this method, first the oil pressure will be solved implicitly, followed by the oil saturation which is calculated explicitly. The next steps contain the mass fractions of the components in both phases to be calculated implicitly.

C.1 OIL PRESSURE EQUATION

Summation of the mass balance equations (3-2) to (3-6) and application of the boundary conditions result in the following material balance for the oil and water phase:

$$\phi \frac{\partial(\rho_o S_o)}{\partial t} = -\frac{\partial(u_o \rho_o)}{\partial x} + U \qquad (C\text{-}1)$$

$$\phi \frac{\partial(\rho_w S_w)}{\partial t} = -\frac{\partial(u_w \rho_w)}{\partial x} - U \qquad (C\text{-}2)$$

These relations can be expanded to:

$$\phi S_o \frac{\partial \rho_o}{\partial t} + \phi \rho_o \frac{\partial S_o}{\partial t} = -\frac{\partial(u_o \rho_o)}{\partial x} + U \qquad (C\text{-}3)$$

$$\phi S_w \frac{\partial \rho_w}{\partial t} + \phi \rho_w \frac{\partial S_w}{\partial t} = -\frac{\partial(u_w \rho_w)}{\partial x} - U \qquad (C\text{-}4)$$

Divide the density of oil for the oil equation (C-3) and water (C-4) for the water equation, then summation of the resultant equations will be:

$$\phi \frac{S_o}{\rho_o} \frac{\partial \rho_o}{\partial t} + \phi \frac{S_w}{\rho_w} \frac{\partial \rho_w}{\partial t} = -\frac{1}{\rho_o} \frac{\partial(u_o \rho_o)}{\partial x} - \frac{1}{\rho_w} \frac{\partial(u_w \rho_w)}{\partial x} + U\left(\frac{1}{\rho_o} - \frac{1}{\rho_w}\right) \qquad (C\text{-}5)$$

The densities are functions of the pressure and composition of the phase:

$$\rho_o = \rho_o(P_o, \omega_o^o, \omega_o^{co_2}) \qquad (C\text{-}6)$$

$$\rho_w = \rho_w(P_w, \omega_w^w, \omega_w^{co_2}) \qquad (C\text{-}7)$$

The density is proportional to the mass fraction of the components, therefore the derivatives of the oil phase and water phase densities with respect to time can be formulated as:

$$\frac{\partial \rho_o}{\partial t} = \sum_{I \in \{o, co_2\}} \varsigma^I \frac{\partial \omega_o^I}{\partial t} + c_o \rho_o \frac{\partial P_o}{\partial t} \quad (C\text{-}8)$$

$$\frac{\partial \rho_w}{\partial t} = \sum_{J \in \{w, co_2\}} \varsigma^J \frac{\partial \omega_w^J}{\partial t} + c_w \rho_w \frac{\partial P_w}{\partial t} \quad (C\text{-}9)$$

Here 'ζ' is the density of the pure substance. Substitute this in the simplified material balance (C-5) and this will result in the following equation:

$$\begin{aligned} &\phi S_o c_o \frac{\partial P_o}{\partial t} + \phi S_w c_w \frac{\partial P_w}{\partial t} + \phi \frac{S_o}{\rho_o} \sum_{I \in \{o, co_2\}} \varsigma^I \frac{\partial \omega_o^I}{\partial t} + \phi \frac{S_w}{\rho_w} \sum_{J \in \{w, co_2\}} \varsigma^J \frac{\partial \omega_w^J}{\partial t} \\ &= -\frac{1}{\rho_o} \frac{\partial (u_o \rho_o)}{\partial x} - \frac{1}{\rho_w} \frac{\partial (u_w \rho_w)}{\partial x} + U\left(\frac{1}{\rho_o} - \frac{1}{\rho_w}\right) \end{aligned} \quad (C\text{-}10)$$

With the use of Darcy's law ((3-7) and (3-8)) and the capillary pressure equation (**Fout! Verwijzingsbron niet gevonden.**, **Fout! Verwijzingsbron niet gevonden.** and **Fout! Verwijzingsbron niet gevonden.**, rearrangement of the previous equation (C-10) yields:

$$\begin{aligned} &\phi (S_o c_o + S_w c_w) \frac{\partial P_o}{\partial t} - \frac{1}{\rho_o} \frac{\partial}{\partial x} \left(\rho_o \lambda_o \frac{\partial P_o}{\partial x}\right) - \frac{1}{\rho_w} \frac{\partial}{\partial x} \left(\rho_w \lambda_w \frac{\partial P_o}{\partial x}\right) \\ &= -\phi \frac{S_o}{\rho_o} \sum_{I \in \{o, co_2\}} \varsigma^I \frac{\partial \omega_o^I}{\partial t} - \phi \frac{S_w}{\rho_w} \sum_{J \in \{w, co_2\}} \varsigma^J \frac{\partial \omega_w^J}{\partial t} \\ &+ U\left(\frac{1}{\rho_o} - \frac{1}{\rho_w}\right) - \frac{1}{\rho_w} \frac{\partial}{\partial x} \left(\rho_w \lambda_w \frac{\partial P_c}{\partial x}\right) \end{aligned} \quad (C\text{-}11)$$

C.2 Discretization of the Pressure Equation

For the capillary pressure for the time derivative of oil pressure a backward difference is used but for other time derivatives a forward difference is chosen. Assume that the length of the grid blocks is the same and equal. Another assumption is that those properties of each grid block which are related to flow, are taken from the previous block. These properties are relative permeability and fluid density. The subscript 'i' represents the grid block number and the superscript 'n' represents the time step. Numerically discretized forms of the terms appearing in the equation are:

$$\frac{\partial P_o}{\partial t} = \frac{P_{o,i}^{n+1} - P_{o,i}^{n}}{\Delta t} \tag{C-12}$$

$$\begin{aligned}\frac{1}{\rho_o}\frac{\partial}{\partial x}(-\rho_o\lambda_o\frac{\partial P_o^{n+1}}{\partial x}) &= \frac{1}{\rho_{o,i}}\frac{(-\rho_o\lambda_o\frac{\partial P_o^{n+1}}{\partial x})_{i+1/2} - (-\rho_o\lambda_o\frac{\partial P_o^{n+1}}{\partial x})_{i-1/2}}{\Delta x} \\ &= -\frac{1}{\rho_{o,i}}\frac{(\rho_o\lambda_o)_i^n\frac{P_{o,i+1}^{n+1} - P_{o,i}^{n+1}}{\Delta x} - (\rho_o\lambda_o)_{i-1}^n\frac{P_{o,i}^{n+1} - P_{o,i-1}^{n+1}}{\Delta x})}{\Delta x}\end{aligned} \tag{C-13}$$

For each component 'i' in each phase is valid:

$$\frac{\partial \omega_\alpha^I}{\partial t} = \frac{\omega_{\alpha,i}^{I,n} - \omega_{\alpha,i}^{I,n-1}}{\Delta t} \tag{C-14}$$

For the initialization at t = 0 seconds:

$$\frac{\partial \omega_o^I}{\partial t} = 0 \tag{C-15}$$

Substituting (C-12) and (C-14)into equation (C-11) gives:

$$\begin{aligned}&\phi(S_o c_o + S_w c_w)_i^n\frac{P_{o,i}^{n+1} - P_{o,i}^{n}}{\Delta t} - \frac{1}{\rho_{o,i}^n}\left[(\rho_o\lambda_o)_i^n\frac{P_{o,i+1}^{n+1} - P_{o,i}^{n+1}}{\Delta x^2} - (\rho_o\lambda_o)_{i-1}^n\frac{P_{o,i}^{n+1} - P_{o,i-1}^{n+1}}{\Delta x^2}\right] \\ &-\frac{1}{\rho_{w,i}^n}\left[(\rho_w\lambda_w)_i^n\frac{P_{o,i+1}^{n+1} - P_{o,i}^{n+1}}{\Delta x^2} - (\rho_w\lambda_w)_{i-1}^n\frac{P_{o,i}^{n+1} - P_{o,i-1}^{n+1}}{\Delta x^2}\right] \\ &= -\frac{1}{\rho_{w,i}^n}\left[(\rho_w\lambda_w)_i^n\frac{P_{c,i+1}^{n} - P_{c,i}^{n}}{\Delta x^2} - (\rho_w\lambda_w)_{i-1}^n\frac{P_{c,i+1}^{n} - P_{c,i-1}^{n}}{\Delta x^2}\right] \\ &-\phi\left(\frac{\partial S_o}{\rho_o}\right)_i^n\sum_{I\in\{o,co_2\}}\varsigma_i^{I,n}\frac{\omega_{o,i}^{I,n} - \omega_{o,i}^{I,n-1}}{\Delta t} - \phi\left(\frac{S_w}{\rho_w}\right)_i^n\sum_{J\in\{w,co_2\}}\varsigma^{J,n}\frac{\omega_{w,i}^{J,n} - \omega_{w,i}^{J,n-1}}{\Delta t} \\ &+U_i^n(\frac{1}{\rho_{o,i}^n} - \frac{1}{\rho_{w,i}^n})\end{aligned} \tag{C-16}$$

The unknown oil pressure can be written as:

$$AP_{o,i+1}^{n+1} + BP_{o,i}^{n+1} + CP_{o,i-1}^{n+1} = D \tag{C-17}$$

For the inner grid blocks the system becomes:

$$
\begin{aligned}
A &= -\left(\lambda_{o,i}^{n} + \lambda_{w,i}^{n}\right) \\
B &= \left(\lambda_{o,i}^{n} + \lambda_{w,i}^{n} + \frac{\rho_{o,i-1}^{n}}{\rho_{o,i}^{n}}\lambda_{o,i-1}^{n} + \frac{\rho_{w,i-1}^{n}}{\rho_{w,i}^{n}}\lambda_{w,i-1}^{n}\right) + \frac{\phi\Delta x^{2}}{\Delta t}\left(S_o c_o + S_w c_w\right)_i^{n} \\
C &= -\left(\frac{\rho_{o,i-1}^{n}}{\rho_{o,i}^{n}}\lambda_{o,i-1}^{n} + \frac{\rho_{w,i-1}^{n}}{\rho_{w,i}^{n}}\lambda_{w,i-1}^{n}\right) \\
D &= \frac{\phi\Delta x^{2}}{\Delta t}\left[\left(S_o c_o + S_w c_w\right)_i^{n} P_{o,i}^{n} - \left(\frac{S_o}{\rho_o}\right)_i^{n}\sum_{I}\varsigma_i^{I,n}\left(\omega_{o,i}^{I,n} - \omega_{o,i}^{I,n-1}\right)\right. \\
&\left. -\left(\frac{S_w}{\rho_w}\right)\sum_{J}\varsigma_i^{J,n}\left(\omega_{w,i}^{J,n} - \omega_{w,i}^{J,n-1}\right)\right] \\
&-\lambda_{w,i}^{n}\left(P_{c,i+1}^{n} - P_{c,i}^{n}\right) + \frac{\rho_{w,i-1}^{n}}{\rho_{w,i}^{n}}\lambda_{w,i-1}^{n}\left(P_{c,i}^{n} - P_{c,i-1}^{n}\right) + \Delta x^{2}\left(\frac{1}{\rho_{o,i}^{n}} - \frac{1}{\rho_{w,i}^{n}}\right)U_i^{n}
\end{aligned}
\qquad \text{(C-18)}
$$

In order to compute the boundary conditions, two imaginary grid blocks are introduced, a grid block '0' which is assumed to be adjacent to the first grid block. Here the injection rate boundary condition is modeled. And the other imaginary grid block is grid block 'n+1' which is adjacent to the last grid block. Here the extrapolated water saturation is modeled.

According to Darcy's law at each time step at the inlet:

$$
\begin{aligned}
&A^{*}\lambda_{\alpha}\frac{\partial P_{\alpha}}{\partial x} = -q_{\alpha}\frac{\rho_{\alpha,sc}}{\rho_{\alpha}} \Rightarrow P_{\alpha,1} - P_{\alpha,0} = -\frac{q_{\alpha}\Delta x\rho_{\alpha,sc}}{A^{*}\lambda_{\alpha}\rho_{\alpha}} \Rightarrow P_{o,1} - P_{o,0} = -\frac{q_o\rho_{o,sc}\Delta x}{A^{*}\rho_o\lambda_o} \\
&\Rightarrow P_{w,1} - P_{w,0} = -\frac{q_w\rho_{w,sc}\Delta x}{A^{*}\rho_w\lambda_w} \Rightarrow P_{c,1} - P_{c,0} = -\frac{q_o\rho_{o,sc}\Delta x}{A^{*}\rho_o\lambda_o} + \frac{q_w\rho_{w,sc}\Delta x}{A^{*}\rho_w\lambda_w}
\end{aligned}
\qquad \text{(C-19)}
$$

For grid block 1 is valid:

$$
A_1 P_{o,2}^{n+1} + \left(B_1 + C_1\right)P_{o,1}^{n+1} = D_1 - C_1\frac{q_o\rho_{o,sc}\Delta x}{A^{*}\rho_o\lambda_o} \qquad \text{(C-20)}
$$

Substituting equation (C-19) into the last equation (C-20) results in:

$$
A_1 P_{o,2}^{n+1} + \left(B_1 + C_1\right)P_{o,1}^{n+1} = D_1 - C_1\frac{q_o\rho_{o,sc}\Delta x}{A^{*}\rho_o\lambda_o} \qquad \text{(C-21)}
$$

The coefficients are obtained as:

$$
\begin{aligned}
A_1 &= -\left(\lambda_{o,1}^n + \lambda_{w,1}^n\right) \\
B_1 &= 2\left(\lambda_{o,1}^n + \lambda_{w,1}^n\right) + \frac{\phi \Delta x^2}{\Delta t}\left(S_o c_o + S_w c_w\right)_1^n \\
C_1 &= -\left(\lambda_{o,1}^n + \lambda_{w,1}^n\right) \\
D_1 &= \frac{\phi \Delta x^2}{\Delta t}\left[\left(S_o c_o + S_w c_w\right)_1^n P_{o,1}^n - \left(\frac{S_o}{\rho_o}\right)_1^n \sum_I \varsigma_1^{I,n}\left(\omega_{o,1}^{I,n} - \omega_{o,1}^{I,n-1}\right)\right. \\
&\left. - \left(\frac{S_w}{\rho_w}\right)_1^n \sum_J \varsigma_1^{J,n}\left(\omega_{w,1}^{J,n} - \omega_{w,1}^{J,n-1}\right)\right] \\
&- \lambda_{w,1}^n\left(P_{c,2}^n - P_{c,1}^n\right) + \frac{\Delta x}{\rho_{w,1}^n A^*}\left(-\frac{q_o \rho_w \lambda_w \rho_{o,sc}}{\rho_o \lambda_o} + q_w \rho_{w,sc}\right)_1^n + \Delta x^2\left(\frac{1}{\rho_{o,1}^n} - \frac{1}{\rho_{w,1}^n}\right) U_1^n
\end{aligned}
\qquad \text{(C-22)}
$$

For the outlet a different boundary condition is used. The water saturation in imaginary grid block 'n+1' is calculated as stated in Table 3-1. This fixes the capillary pressure at the outlet:

$$
\begin{aligned}
&P_\alpha(x = L) = P_{outflow} \Rightarrow P_{o,N+1} - P_{o,N} = 2\left(P_{outflow} - P_{o,N}\right) \\
&\Rightarrow P_{o,N+1} = 2P_{outflow} - P_{o,N}
\end{aligned}
\qquad \text{(C-23)}
$$

Here '$P_{outflow}$' is the pressure of the water in the outlet. The oil pressure can be calculated with the capillary pressure equation **Fout! Verwijzingsbron niet gevonden.** and the water pressure. With use of equation (C-23) for the outlet can be written:

$$
(B_N - A_N)P_{o,N}^{n+1} + C_N P_{o,N-1}^{n+1} = D_N - 2A_N P_{outflow}
\qquad \text{(C-24)}
$$

In which the coefficients are obtained as:

$$
\begin{aligned}
A_N &= -\left(\lambda_{o,N}^n + \lambda_{w,N}^n\right) \\
B_N &= \left(\lambda_{o,N}^n + \lambda_{w,N}^n + \frac{\rho_{o,N-1}^n}{\rho_{o,N}^n}\lambda_{o,N-1}^n + \frac{\rho_{w,N-1}^n}{\rho_{w,N}^n}\lambda_{w,N-1}^n\right) + \frac{\phi \Delta x^2}{\Delta t}\left(S_o c_o + S_w c_w\right)_N^n \\
C_N &= -\left(\frac{\rho_{o,N-1}^n}{\rho_{o,N}^n}\lambda_{o,N-1}^n + \frac{\rho_{w,N-1}^n}{\rho_{w,N}^n}\lambda_{w,N-1}^n\right) \\
D_N &= \frac{\phi \Delta x^2}{\Delta t}\left[\left(S_o c_o + S_w c_w\right)_N^n P_{o,N}^n - \left(\frac{S_o}{\rho_o}\right)_N^n \sum_I \varsigma_N^{I,n}\left(\omega_{o,N}^{I,n} - \omega_{o,N}^{I,n-1}\right)\right. \\
&\left. - \left(\frac{S_w}{\rho_w}\right)_N^n \sum_J \varsigma_N^{J,n}\left(\omega_{w,N}^{J,n} - \omega_{w,N}^{J,n-1}\right)\right] \\
&+ \lambda_{w,N}^n P_{c,N}^n + \frac{\rho_{w,N-1}^n}{\rho_{w,N}^n}\lambda_{w,N-1}^n\left(P_{c,N}^n - P_{c,N-1}^n\right) + \Delta x^2\left(\frac{1}{\rho_{o,N}^n} - \frac{1}{\rho_{w,N}^n}\right) U_N^n
\end{aligned}
\qquad \text{(C-25)}
$$

C.3 Explicit Saturation Calculation

After the pressure equation has been solved, the oil saturation will be updated using equation (C-1). In this stage all variables but pressures are still being calculated explicitly. Discretization of equation (C-1) shows:

$$\phi\frac{\partial(\rho_o S_o)}{\partial t}=-\frac{\partial(u_o\rho_o)}{\partial x}+U$$

$$discretization\Rightarrow$$

$$\frac{\phi}{\Delta t}\left(\rho_{o,i}^{n+1}S_{o,i}^{n+1}-\rho_{o,1}^{n}S_{o,i}^{n}\right)=\left[\left(\rho_o\lambda_o\right)_i^n\frac{P_{o,i+1}^{n+1}-P_{o,i}^{n+1}}{\Delta x^2}-\left(\rho_o\lambda_o\right)_{i-1}^n\frac{P_{o,i}^{n+1}-P_{o,i-1}^{n+1}}{\Delta x^2}\right]+U_i^n \qquad (C\text{-}26)$$

$$or\Rightarrow S_{o,i}^{n+1}=\frac{\rho_{o,i}^n}{\rho_{o,i}^{n+1}}S_{o,i}^n+\frac{\Delta t}{\phi\rho_{o,i}^{n+1}}\left[\left(\rho_o\lambda_o\right)_i^n\frac{P_{o,i+1}^{n+1}-P_{o,i}^{n+1}}{\Delta x^2}-\left(\rho_o\lambda_o\right)_{i-1}^n\frac{P_{o,i}^{n+1}-P_{o,i-1}^{n+1}}{\Delta x^2}+U_i^n\right]$$

And for the boundary grid points the oil saturation will be obtained by:

$$S_{o,1}^{n+1}=\frac{\rho_{o,1}^n}{\rho_{o,1}^{n+1}}S_{o,1}^n+\frac{\Delta t}{\phi\rho_{o,1}^{n+1}}\left[\left(\rho_o\lambda_o\right)_1^n\frac{P_{o,2}^{n+1}-P_{o,1}^{n+1}}{\Delta x^2}+\frac{q_o\rho_{o,sc}}{\Delta xA^*}+U_1^n\right] \qquad (C\text{-}27)$$

$$S_{o,N}^{n+1}=\frac{\rho_{o,N}^n}{\rho_{o,N}^{n+1}}S_{o,N}^n+\frac{\Delta t}{\phi\rho_{o,N}^{n+1}}\left[2\left(\rho_o\lambda_o\right)_N^n\frac{P_{o,outflow}-P_{o,N}^{n+1}}{\Delta x^2}-\left(\rho_o\lambda_o\right)_{N-1}^n\frac{P_{o,N}^{n+1}-P_{o,N-1}^{n+1}}{\Delta x^2}+U_N^n\right] \qquad (C\text{-}28)$$

C.4 Explicit Darcy Velocity Calculation

According to Darcy's law, 'u' depends mostly on saturation and pressure. Having updated these parameters, 'u' can be updated directly. This is useful in order to make the following discretization shorter and faster. The Darcy velocity in the grid blocks is calculated:

$$u_{\alpha,i}^{n+1}=-\frac{1}{\Delta x}\lambda_{\alpha,i}^{n+1}\left(P_{\alpha,i+1}^{n+1}-P_{\alpha,i}^{n+1}\right) \qquad (C\text{-}29)$$

And for the boundary conditions:

$$\begin{aligned}&u_{\alpha,0}^{n+1}=u_{\alpha,inj}^{n+1}=\frac{q_\alpha}{A^*}\frac{\rho_{\alpha,sc}}{\rho_\alpha^{n+1}};\\&u_{\alpha,N}^{n+1}=-\frac{2}{\Delta x}\lambda_{\alpha,N}^{n+1}\left(P_{outflow}-P_{\alpha,N}^{n+1}\right)\end{aligned} \qquad (C\text{-}30)$$

C.5 Implicit Composition Calculation

The water phase composition is updated by using the mass balance equation for water in the water phase. For the inner grid blocks and the outlet is valid:

$$\phi\frac{\partial\left(\rho_w S_w \omega_w^w\right)}{\partial t} = -\frac{\left(u_w \rho_w \omega_w^w\right)}{\partial x}$$

$$discretization \Rightarrow$$

$$\left(\rho_w S_w \omega_w^w\right)_i^{n+1} - \left(\rho_w S_w \omega_w^w\right)_i^n = -\frac{\Delta t}{\phi \Delta x}\left(\rho_{w,i}^{n+1} u_{w,i}^{n+1} \omega_{w,i}^{n+1} - \rho_{w,i-1}^{n+1} u_{w,i-1}^{n+1} \omega_{w,i-1}^{n+1}\right) \quad (C\text{-}31)$$

$$rearrangement \Rightarrow$$

$$\left[\rho_{w,i}^{n+1} S_{w,i}^{n+1} + \frac{\Delta t}{\phi \Delta x}\rho_{w,i}^{n+1} u_{w,i}^{n+1}\right]\omega_{w,i}^{w,n+1} - \left[\frac{\Delta t}{\phi \Delta x}\rho_{w,i-1}^{n+1} u_{w,i-1}^{n+1}\right]\omega_{w,i-1}^{w,n+1} = \rho_{w,i}^n S_{w,i}^n \omega_{w,i}^n$$

For the inlet:

$$\left[\rho_{w,1}^{n+1} S_{w,1}^{n+1} + \frac{\Delta t}{\phi \Delta x}\rho_{w,1}^{n+1} u_{w,1}^{n+1}\right]\omega_{w,1}^{w,n+1} - \left[\frac{\Delta t}{\phi \Delta x}\rho_{w,inj}^{n+1} u_{w,inj}^{n+1}\right]\omega_{w,inj}^{w,n+1} = \rho_{w,1}^n S_{w,1}^n \omega_{w,1}^{w,n}$$

$$simplified \Rightarrow \quad (C\text{-}32)$$

$$\left[\rho_{w,1}^{n+1} S_{w,1}^{n+1} + \frac{\Delta t}{\phi \Delta x}\rho_{w,1}^{n+1} u_{w,1}^{n+1}\right]\omega_{w,1}^{w,n+1} = \rho_{w,1}^n S_{w,1}^n \omega_{w,1}^{w,n} + \frac{\Delta t}{\phi \Delta x}\rho_{w,inj}^{n+1} u_{w,inj}^{n+1} \omega_{w,inj}^{w,n+1}$$

Where '$\omega_{w,injected}$' is the mass fraction of water in the water phase. The mass fraction of CO2 in the water can be obtained from its mass balance equation in the water phase. The resultant equation is:

$$\left[\rho_{w,i}^{n+1} S_{w,i}^{n+1} + \frac{\Delta t}{\phi \Delta x}\rho_{w,i}^{n+1} u_{w,i}^{n+1}\right]\omega_{w,i}^{co_2,n+1} - \left[\frac{\Delta t}{\phi \Delta x}\rho_{w,i-1}^{n+1} u_{w,i-1}^{n+1}\right]\omega_{w,i-1}^{co_2,n+1} = \rho_{w,i}^n S_{w,i}^n \omega_{w,i}^{CO_2,n} - U(i) \quad (C\text{-}33)$$

For the oil a similar construction is possible:

$$\phi\frac{\partial\left(\rho_o S_o \omega_o^o\right)}{\partial t} = -\frac{\partial\left(u_o \rho_o \omega_o^o\right)}{\partial x} + U$$

$$discretize \Rightarrow \quad (C\text{-}34)$$

$$\left(\frac{\phi}{\Delta t}\rho_o S_o + \frac{1}{\Delta x}u_o \rho_o\right)_i^{n+1} \omega_{o,i}^{co_2,n+1} - \frac{1}{\Delta x}\left(u_o \rho_o\right)_{i-1}^{n+1} \omega_{o,i-1}^{co_2,n+1} = \frac{\phi}{\Delta t}\left(\rho_o S_o \omega_o^{co_2}\right)_i^n + U_i^n$$

The composition of oil in the oil phase can be updated in the same way implicitly using the following discretized equation:

$$\left(\frac{\phi}{\Delta t}\rho_o S_o + \frac{1}{\Delta x}u_o \rho_o\right)_i^{n+1} \omega_{o,i}^{o,n+1} - \frac{1}{\Delta x}\left(u_o \rho_o\right)_{i-1}^{n+1} \omega_{o,i-1}^{o,n+1} = \frac{\phi}{\Delta t}\left(\rho_o S_o \omega_o^o\right)_i^n \quad (C\text{-}35)$$

Some equations here are missing (CO2 in oil and CO2 in water)

D. APPENDIX ON MASS TRANSFER

D.1 MASS TRANSFER FOR LOW OIL SATURATIONS

The porosity according to the model can be obtained as follows:

$$\phi = \frac{m\pi r_w^2}{A} = \frac{MA\pi r_w^2}{A} = M\pi r_w^2 \Rightarrow M = \frac{\phi}{\pi r_w^2} \qquad (D\text{-}1)$$

In which 'm' is the number of tubes, 'M' is the number of tubes per unit area of the cross section, and 'r_w' denotes the outer radius of pore water ring around the oil blobs. Further it van be claimed that:

$$\sigma = \frac{2\pi r_o l(MA)}{l} = 2\pi r_o(MA) \qquad (D\text{-}2)$$

Where 'l' is the length of the core, and 'r_o' is the radius of the oil tube as shown in Figure 3-2. From the last two equations it follows that:

A.1 MASS TRANSFER FOR LOW OIL SATURATIONS

The porosity according to the model can be obtained as follows:

$$\phi = \frac{m\pi r_w^2}{A} = \frac{MA\pi r_w^2}{A} = M\pi r_w^2 \Rightarrow M = \frac{\phi}{\pi r_w^2} \qquad (D\text{-}1)$$

In which 'm' is the number of tubes, 'M' is the number of tubes per unit area of the cross section, and 'r_w' denotes the outer radius of pore water ring around the oil blobs. Further it van be claimed that:

$$\sigma = \frac{2\pi r_o l(MA)}{l} = 2\pi r_o(MA) \qquad (D\text{-}2)$$

Where 'l' is the length of the core, and 'r_o' is the radius of the oil tube as shown in Figure 3-2. From the last two equations it follows that:

$$\sigma = \frac{2\pi r_o A}{r_w^2} \qquad (D\text{-}3)$$

The ratio of 'r_o' and 'r_w' can be expressed in terms of saturation:

$$S_o = \frac{r_o^2}{r_w^2} \qquad (D\text{-}4)$$

And therefore the interfacial area can be written as:

$$\sigma = \frac{2\phi A S_o}{r_o} \qquad (D\text{-}5)$$

$$\sigma = \frac{2\pi r_o A}{r_w^2} \qquad \text{(D-3)}$$

The ratio of 'r_o' and 'r_w' can be expressed in terms of saturation:

$$S_o = \frac{r_o^2}{r_w^2} \qquad \text{(D-4)}$$

And therefore the interfacial area can be written as:

$$\sigma = \frac{2\phi A S_o}{r_o} \qquad \text{(D-5)}$$

The geometry of the proposed model also implies that:

$$\Delta r = \frac{r_w + r_o}{2} \qquad \text{(D-6)}$$

Putting the derived interfacial area 'σ' and 'Δr' into the first equation gives:

A.1 Mass Transfer for Low Oil Saturations

The porosity according to the model can be obtained as follows:

$$\phi = \frac{m\pi r_w^2}{A} = \frac{MA\pi r_w^2}{A} = M\pi r_w^2 \Rightarrow M = \frac{\phi}{\pi r_w^2} \qquad \text{(D-1)}$$

In which 'm' is the number of tubes, 'M' is the number of tubes per unit area of the cross section, and 'r_w' denotes the outer radius of pore water ring around the oil blobs. Further it van be claimed that:

$$\sigma = \frac{2\pi r_o l(MA)}{l} = 2\pi r_o (MA) \qquad \text{(D-2)}$$

Where 'l' is the length of the core, and 'r_o' is the radius of the oil tube as shown in Figure 3-2. From the last two equations it follows that:

$$\sigma = \frac{2\pi r_o A}{r_w^2} \qquad \text{(D-3)}$$

The ratio of 'r_o' and 'r_w' can be expressed in terms of saturation:

$$S_o = \frac{r_o^2}{r_w^2} \qquad \text{(D-4)}$$

And therefore the interfacial area can be written as:

$$\sigma = \frac{2\phi A S_o}{r_o} \qquad \text{(D-5)}$$

$$U = \frac{2J\phi S_o}{r_o} = \frac{2D\phi S_o}{r_o \Delta r} \Delta C^{CO_2} \quad \text{(D-7)}$$

'$r_o \Delta r$' is:

$$r_o \Delta r = \frac{2r_o^2 + r_w r_o}{2} = \frac{1}{2} r_w^2 ((\frac{r_o}{r_w})^2 + \frac{r_o}{r_w}) = \frac{1}{2} r_w^2 (S_o + S_o^{1/2}) \quad \text{(D-8)}$$

D.2 Mass Transfer for High Oil Saturations

The porosity according to the model can be obtained as follows:

$$\phi = \frac{mA_{pore}}{A_{core}} = \frac{MA_{core}A_{pore}}{A_{core}} = MA_{pore} \Rightarrow M = \frac{\phi}{A_{pore}} \quad \text{(D-9)}$$

In which 'm' is the number of tubes, 'M' is the number of tubes per unit area of the cross section, and 'A_{pore}' denotes the area of a triangular pore around the oil blobs. Further it van be claimed that:

$$\sigma = \frac{3l_{side}l_{core}(MA_{core})}{l_{core}} = 3l_{side}(MA_{core}) = 3l_{side}\frac{\phi}{A_{pore}}A_{core} \quad \text{(D-10)}$$

In this equation 'l_{side}' is a function of saturation. The relation for this length can be seen below:

A.1 Mass Transfer for Low Oil Saturations

The porosity according to the model can be obtained as follows:

$$\phi = \frac{m\pi r_w^2}{A} = \frac{MA\pi r_w^2}{A} = M\pi r_w^2 \Rightarrow M = \frac{\phi}{\pi r_w^2} \quad \text{(D-1)}$$

In which 'm' is the number of tubes, 'M' is the number of tubes per unit area of the cross section, and 'r_w' denotes the outer radius of pore water ring around the oil blobs. Further it van be claimed that:

$$\sigma = \frac{2\pi r_o l(MA)}{l} = 2\pi r_o(MA) \quad \text{(D-2)}$$

Where 'l' is the length of the core, and 'r_o' is the radius of the oil tube as shown in Figure 3-2. From the last two equations it follows that:

$$\sigma = \frac{2\pi r_o A}{r_w^2} \quad \text{(D-3)}$$

The ratio of 'r_o' and 'r_w' can be expressed in terms of saturation:

$$S_o = \frac{r_o^2}{r_w^2} \quad \text{(D-4)}$$

And therefore the interfacial area can be written as:

$$\sigma = \frac{2\phi A S_o}{r_o} \quad \text{(D-5)}$$

$$l_{side}^{\ 2} = \frac{A_{smalltriangle} \cdot 4}{\tan(60)} = \frac{4(A_{pore}S_w)}{3\tan(60)} \Rightarrow l_{side} = \sqrt{\frac{4(A_{pore}S_w)}{3\tan(60)}} \quad \text{(D-11)}$$

The geometry of the proposed model also implies that:

$$\Delta r = \frac{r_w + r_o}{2} = \frac{4(A_{pore}S_w)}{3l_{side}} + \frac{4A_{pore}}{l_{sidepore}} \quad \text{(D-12)}$$

In this equation 'r_o' and 'r_w' denote the height of the water triangle and the height of the pore triangle. The first one is a function of saturation. Putting the derived interfacial area 'σ' and 'Δr' into the first equation gives:

$$U = D\left(\frac{3l_{side}}{4(A_{pore}S_w)} + \frac{l_{sidepore}}{4A_{pore}}\right)\frac{3l_{side}\phi}{A_{pore}}(\rho_o\omega_o^{co_2} - \rho_w\omega_w^{co_2}) \quad \text{(D-13)}$$

 Appendix on Mass Transfer

A.1 Mass Transfer for Low Oil Saturations

The porosity according to the model can be obtained as follows:

$$\phi = \frac{m\pi r_w^2}{A} = \frac{MA\pi r_w^2}{A} = M\pi r_w^2 \Rightarrow M = \frac{\phi}{\pi r_w^2} \quad \text{(D-1)}$$

In which 'm' is the number of tubes, 'M' is the number of tubes per unit area of the cross section, and 'r_w' denotes the outer radius of pore water ring around the oil blobs. Further it van be claimed that:

$$\sigma = \frac{2\pi r_o l(MA)}{l} = 2\pi r_o(MA) \quad \text{(D-2)}$$

Where 'l' is the length of the core, and 'r_o' is the radius of the oil tube as shown in Figure 3-2. From the last two equations it follows that:

$$\sigma = \frac{2\pi r_o A}{r_w^2} \quad \text{(D-3)}$$

The ratio of 'r_o' and 'r_w' can be expressed in terms of saturation:

$$S_o = \frac{r_o^2}{r_w^2} \quad \text{(D-4)}$$

And therefore the interfacial area can be written as:

$$\sigma = \frac{2\phi A S_o}{r_o} \quad \text{(D-5)}$$

E. APPENDIX ON THE BASE CASE INPUT

Parameter	Value	Unit
Number of grid blocks	10	[-]
Number of imaginary grid blocks	8	[-]
Core length	0.17	[m]
Core radius	0.019	[m]
Temperature	293.15	[K]
Time step	0.5	[s]
Simulation time	30	[hours]
Water injection rate	1	[ml min^{-1}]
Oil injection rate	0	[ml min^{-1}]
Porosity	0.22	[-]
Permeability	1.2	[darcy]
Oil relative endpoint permeability	1	[-]
Water relative endpoint permeability	0.5	[-]
Initial water saturation	0.73	[-]
Connate water saturation	0.20	[-]
Residual oil saturation	0.27	[-]
Initial oil saturation	0.27	[-]
Initial reservoir pressure	25	[bar]
Outflow pressure	25	[bar]
CO_2 mass fraction in injected water	0.037031	[-]
CO_2 mass fraction in injected oil	0	[-]
Oil reference density	773	[kg m^{-3}]
Water reference density	1020	[kg m^{-3}]
CO_2 reference density	1.98	[kg m^{-3}]
Molar weight oil	227	[g mol^{-1}]
Molar weight water	18	[g mol^{-1}]
Molar weight CO_2	44.01	[g mol^{-1}]
Compressibility oil	1e-10	[pa^{-1}]
Compressibility water	1e-10	[pa^{-1}]
Compressibility CO_2	1e-10	[pa^{-1}]
Oil viscosity	0.003	[pa s]
Water viscosity	0.001	[pa s]
CO_2 viscosity	0.00007	[pa s]
Nissan and Grunberg constant	0	[-]
Diffusion constant	1e-12	[m^2 s^{-1}]
Interfacial tension oil/water	30e-3	[N m^{-1}]
Capillary pressure constant	0.5	[-]
Sorting factor (for capillary pressure)	5	[-]
$\alpha_{\text{maximum solubility}}$	1	[-]

$\alpha_{\text{residual oil function}}$	4	[-]
$\alpha_{\text{oil density}}$	1	[-]

Table E-1: Input parameters in base case model

It may be noticed that the porosity of the model (0.22) is different from the experimentally produced value (0.26). The reason for this is to equalize the total pore volume of the two systems. The pore volume of the experiment is equal to 40.68 milliliter. The pore volume of the experiment with the chosen value is 42.42 milliliter, as calculated in equation (E-1).

$$PV = l \cdot \pi r^2 \cdot \phi \qquad \text{(E-1)}$$

In addition to this the mass fraction of CO_2 dissolved in the injected water is determined with the help of a calculator for CO_2 solubility in water designed by Diamond & Akinfiev (2002).